Supporting Information

Binding of Anions in Triply Interlocked Coordination Catenanes and Dynamic Allostery for Dehalogenation Reaction

Linlin Yang, Xu Jing, Bowen An, Cheng He, Yang Yang and Chunying Duan

Contents

1. Measurements and Materials

All chemicals were of reagent grade quality obtained from commercial sources and used as supplied unless otherwise stated. The solvent MeCN and CH_2Cl_2 were dried and distilled from calcium hydride. The elemental analyses of C, H and N were performed on a Vario ELIII elemental analyzer. ^{1}H NMR, ^{13}C NMR and ^{19}F NMR spectra were measured on a Varian INOVA 500M spectrometer. ESI mass spectra were carried out on a HPLC-Q-Tof MS spectrometer. Uv-vis spectra were measured on a HP 8453 spectrometer. Isothermal Titration Calorimetry (ITC) was performed on a Nano ITC (TA Instruments Inc. – Waters LLC). The fluorescence spectra were measured on JASCO FP-6500. The solution of sulfonate dye, Bu_4N**DSA** (DSA, dansyl acid) was prepared in CH_3CN. The solution of **Tet**-1, Cat-BF_4 and Cat-ClO_4 were all prepared in CH_3CN. 2,2'-bipyridine-5-carbaldehyde[1] and tris(4-aminophenyl)amine (TPA)[2] were synthesized under a dry nitrogen atmosphere by means of a standard Schlenk technique following the reported procedures.

In the main text and related synthetic section:

L = tris-[4-N-(2,2'-bipyridine)-5-ylmethylene-amino)-benzene]-amine (Scheme S1)

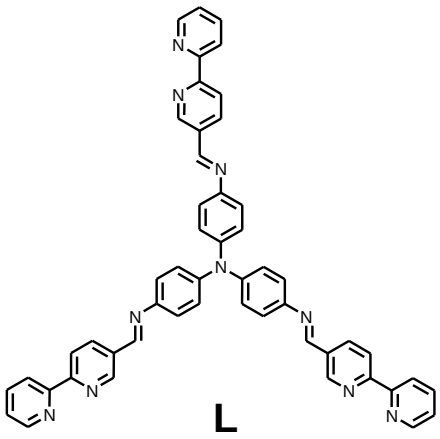

Scheme S1 The molecular structure of ligand L

2. Synthesis and Characterization

2.1 Preparation of interlocked tetrahedron Cat-BF_4 $[Zn_8L_8][BF_4]_{16}$

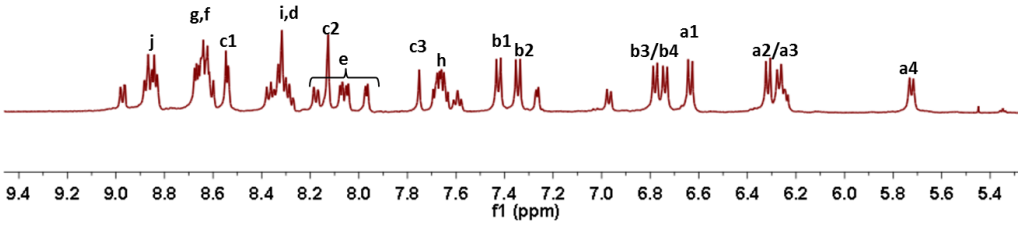

Figure S1. ^{1}H NMR spectrum of **Cat-BF_4** recorded in CD_3CN.

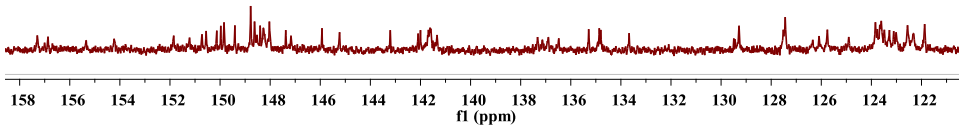

Figure S2. ^{13}C NMR spectrum of **Cat-BF_4** recorded in CD_3CN.

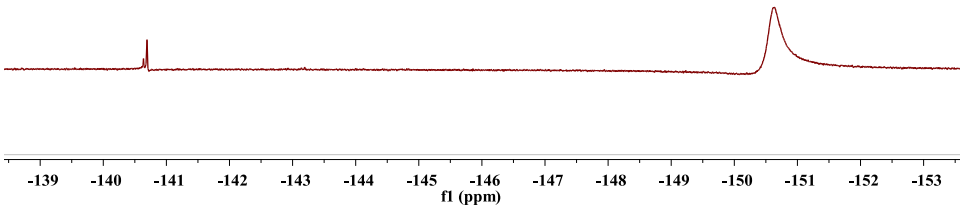

Figure S3. ^{19}F-NMR of **Cat-BF_4** (500MHz, 298K, CD_3CN): δ (ppm) = -140.5 (encapsulated BF_4^-), -150.70 (broad signal, free BF_4^-), indicate the slow anion exchange in outer six pockets.

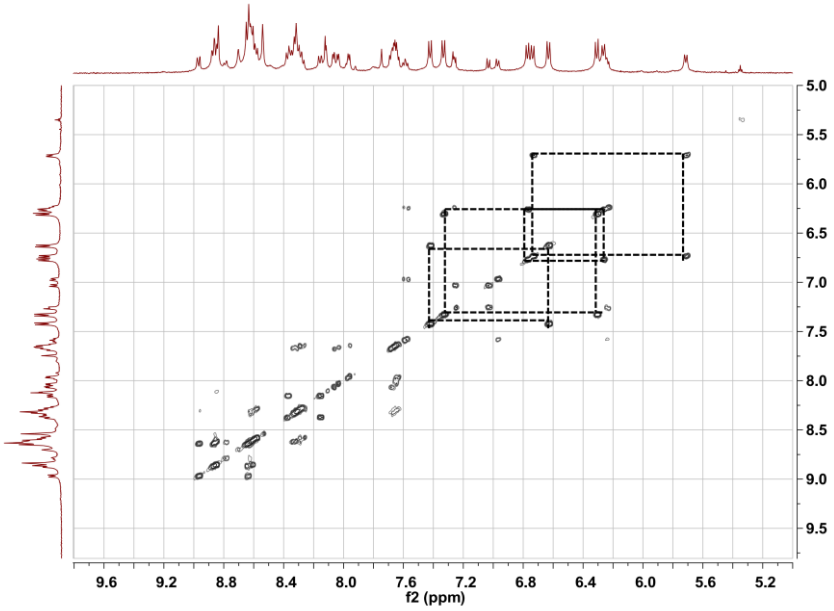

Figure S4. ^{1}H–^{1}H COSY spectrum of **Cat-BF_4** (400 MHz, CD_3CN, 298K).

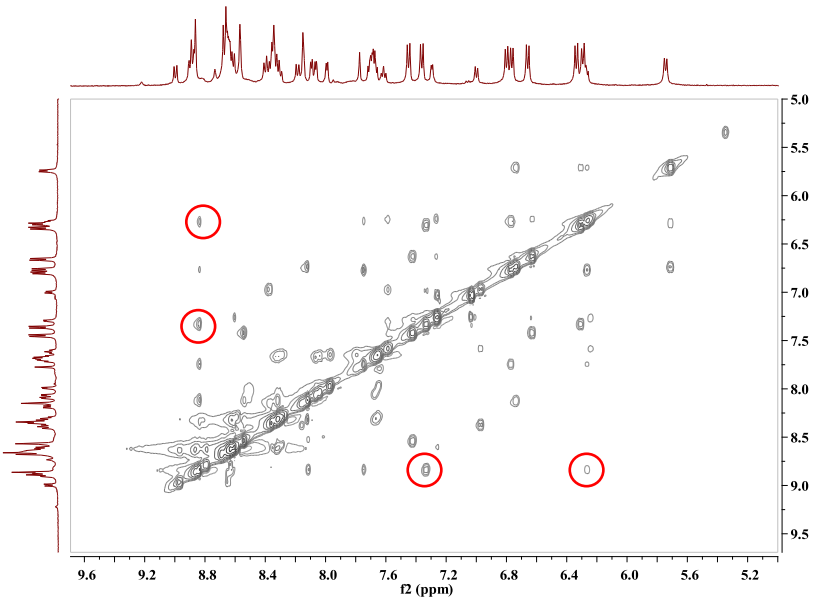

Figure S5. Partial view of ^{1}H-^{1}H NOESY spectra of **Cat-BF_4** recorded in CD_3CN. The H-H interactions between the bipyridyl protons and the TPA protons were found (red cycle). It was due to the interlocked structure which makes the building ligands close to each other.

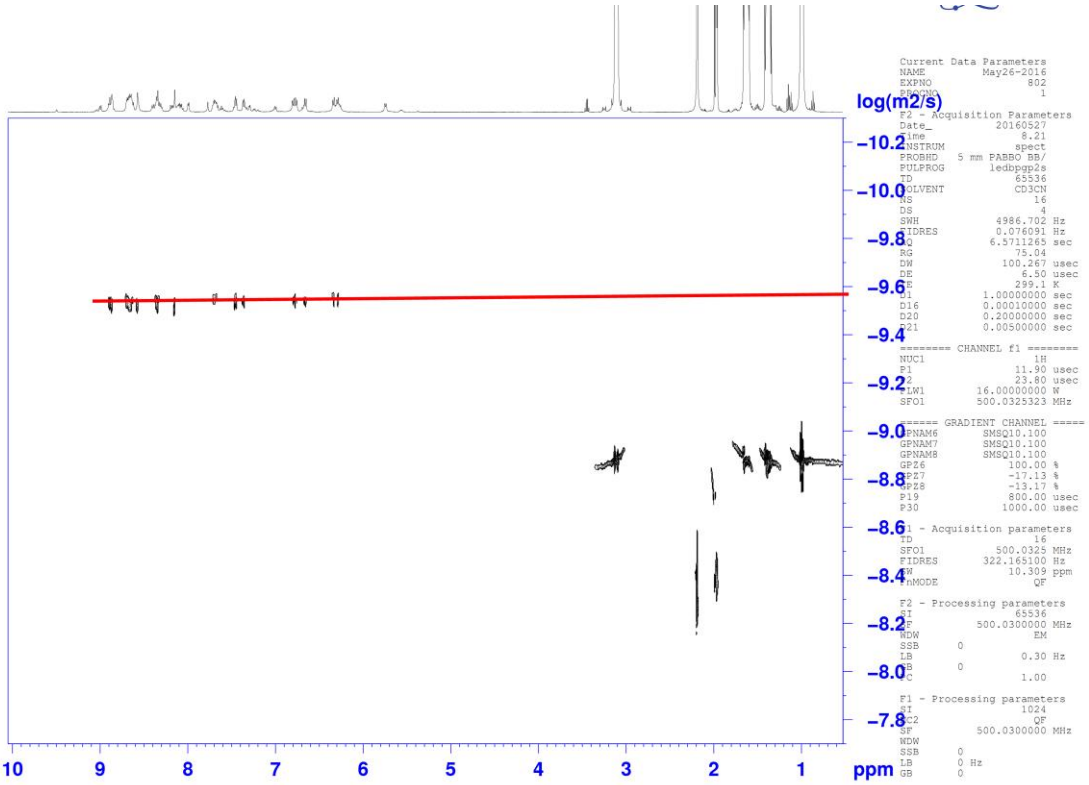

Figure S6. ^{1}H DOSY spectra (500 MHz, 298K, CD_3CN) of **Cat-BF4**. The diffusion coefficient is 2.7×10^{-10} m^2/s.

2.2 Preparation of discrete tetrahedron Tet-1

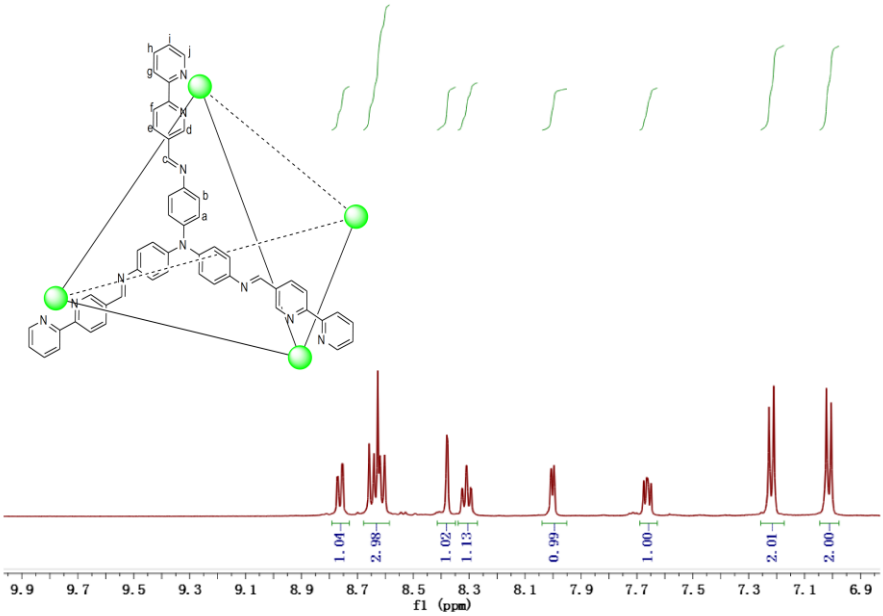

Figure S7. ^{1}H NMR spectrum of **Tet**-1 recorded in CD_3CN.

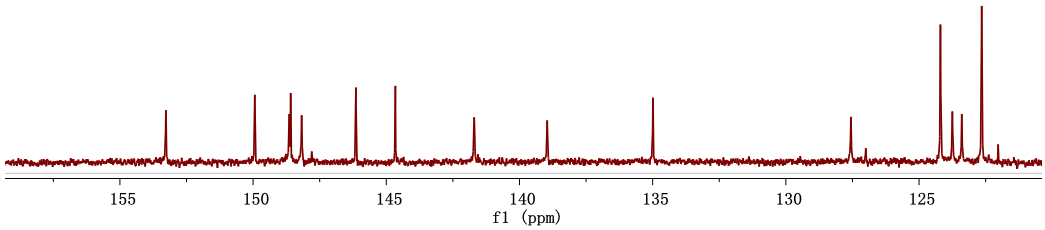

Figure S8. ^{13}C NMR spectrum of **Tet**-1 recorded in CD_3CN.

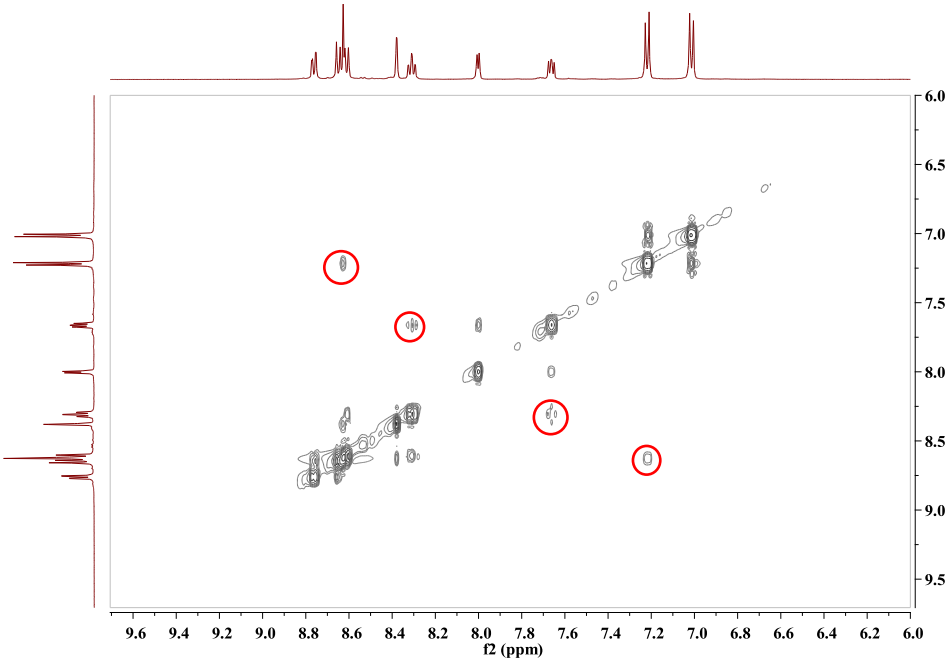

Figure S9. Partial view of ^{1}H–^{1}H NOESY spectra of **Tet**-1 recorded in CD_3CN. An NOE signal was observed between H_d and H_b, but not between H_j and H_b. The fact that H_d points into the inner direction of **Tet**-1 and is proximal to H_b of neighboring ligands indicate that **Tet**-1 is a discrete tetrahedron cage, obeying the face assembly procedure which have been well established.

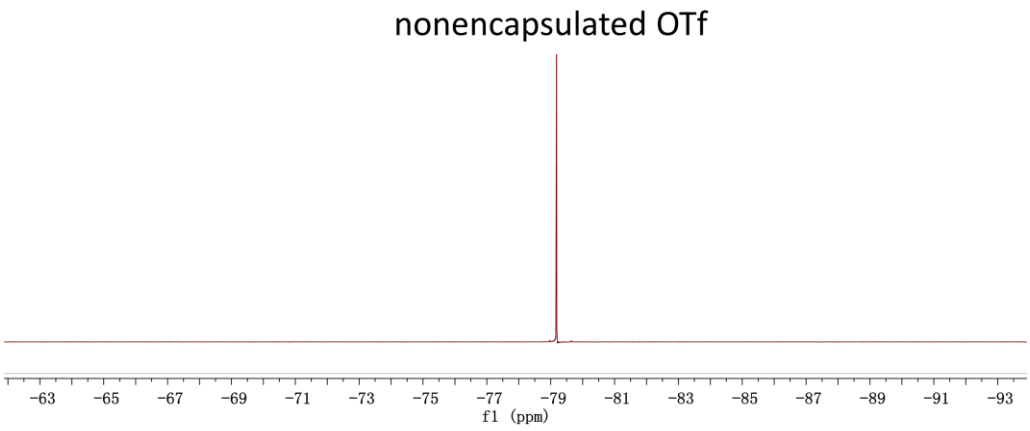

Figure S10. ^{19}F NMR spectrum (CD_3CN, 298K) of **Tet**-1.

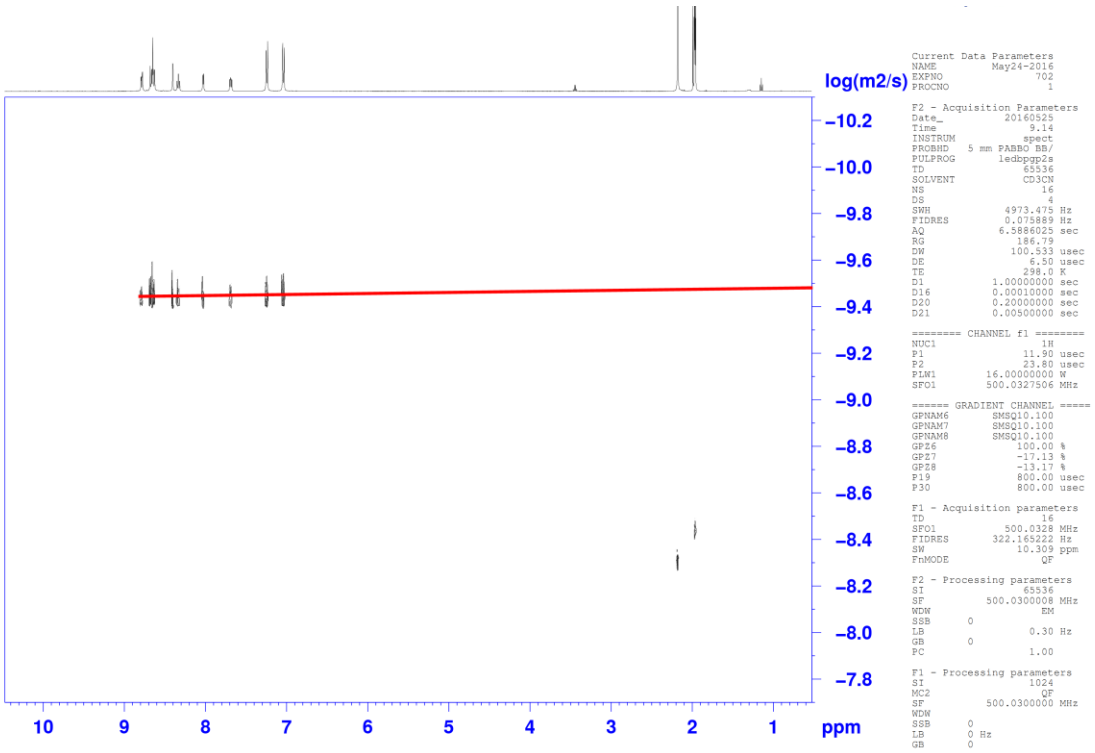

Figure S11. DOSY spectrum (400 MHz, 298K, CD_3CN) for **Tet**-1. The diffusion coefficient is 3.3×10^{-10} m^2/s.

2.3 Preparation of interlocked tetrahedron Cat-ClO_4 $[Zn_8L_8][ClO_4]_{16}$

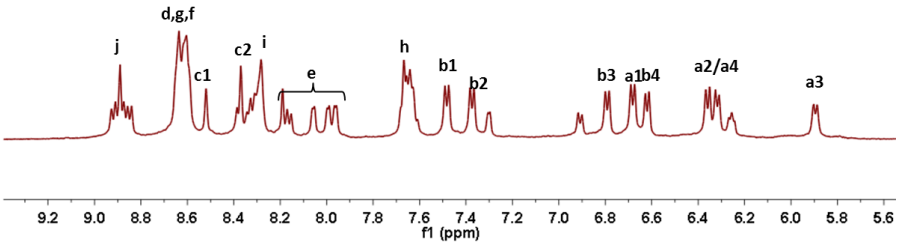

Figure S12. ^{1}H NMR spectrum of interlocked cage **Cat-ClO_4** recorded in CD_3CN.

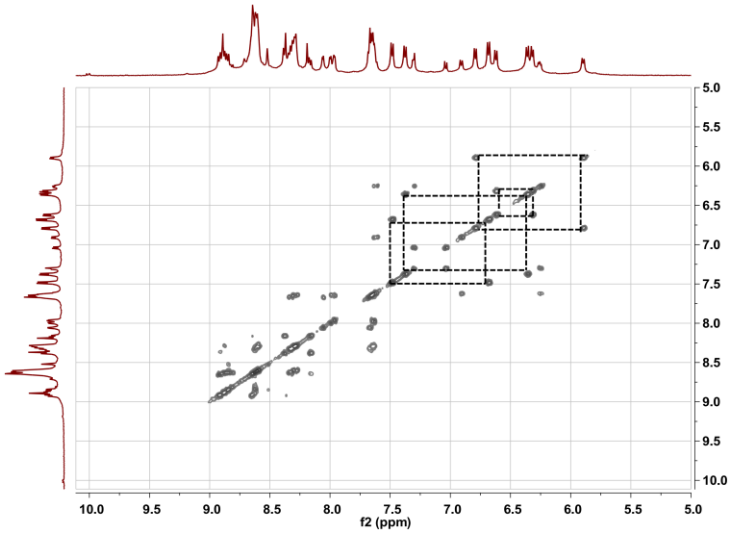

Figure S13. ^{1}H–^{1}H COSY spectrum of **Cat-ClO_4** (400 MHz, CD_3CN, 298K).

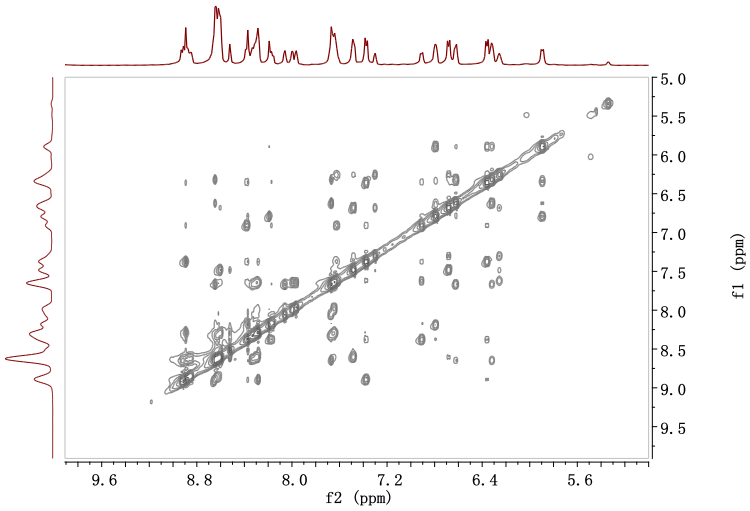

Figure S14. ^{1}H–^{1}H NOESY spectrum of **Cat-ClO_4** recorded in CD_3CN. The complicated H-H interaction was due to the interlocked structure which makes the building ligands close to each other.

2.4 Preparation of interlocked tetrahedron Cat-X (X= Br or I)

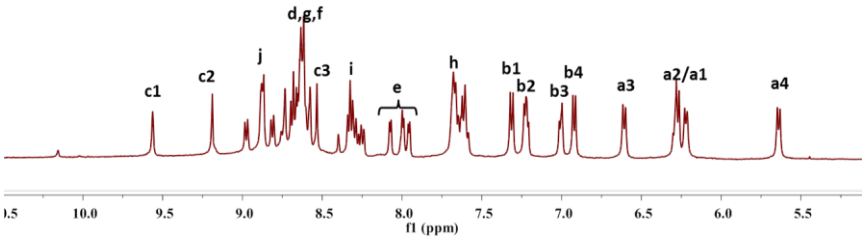

Figure S15. ^{1}H NMR spectrum of **Cat**-Br $[Zn_8L_8][Br]_7$ in CD_3CN at 298K.

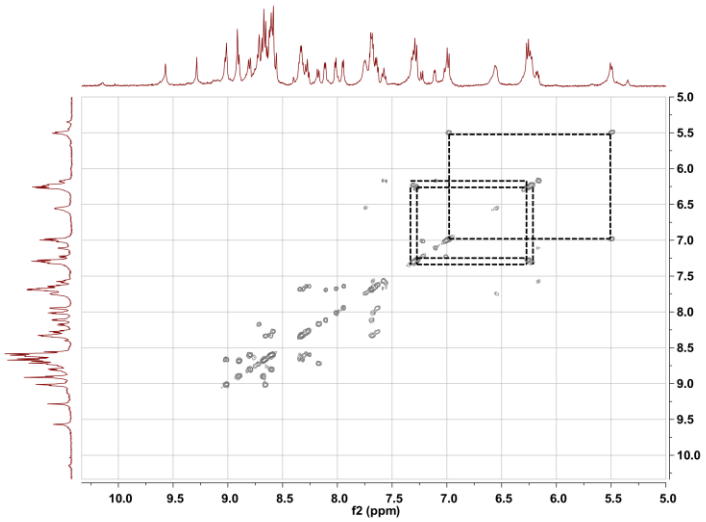

Figure S16. ^{1}H–^{1}H COSY spectrum of **Cat**-Br $[Zn_8L_8][Br]_7$ (400 MHz, CD_3CN, 298K).

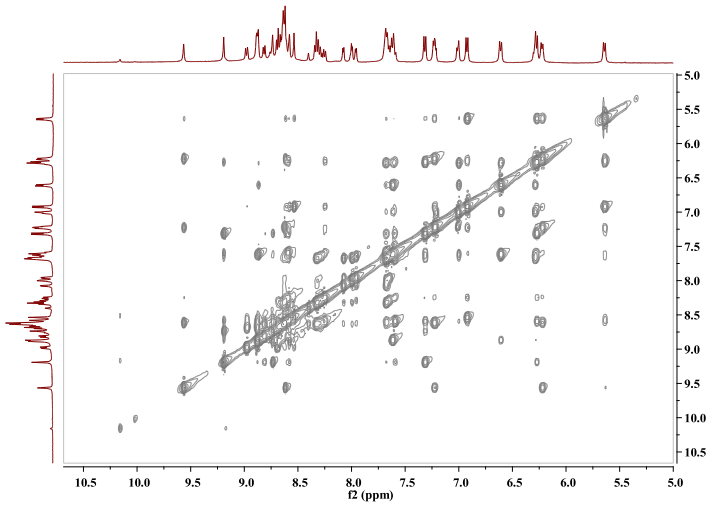

Figure S17. ^{1}H–^{1}H NOESY spectrum of **Cat**-Br $[Zn_8L_8][Br]_7$ (400 MHz, CD_3CN, 298K).

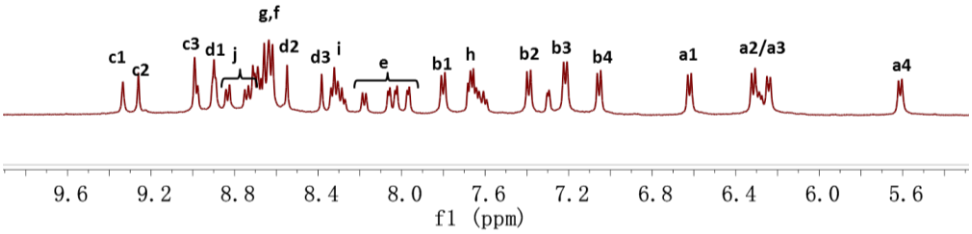

Figure S18. ^{1}H NMR spectrum of **Cat**-I $[Zn_8L_8][I]_7$ in CD_3CN at 298K.

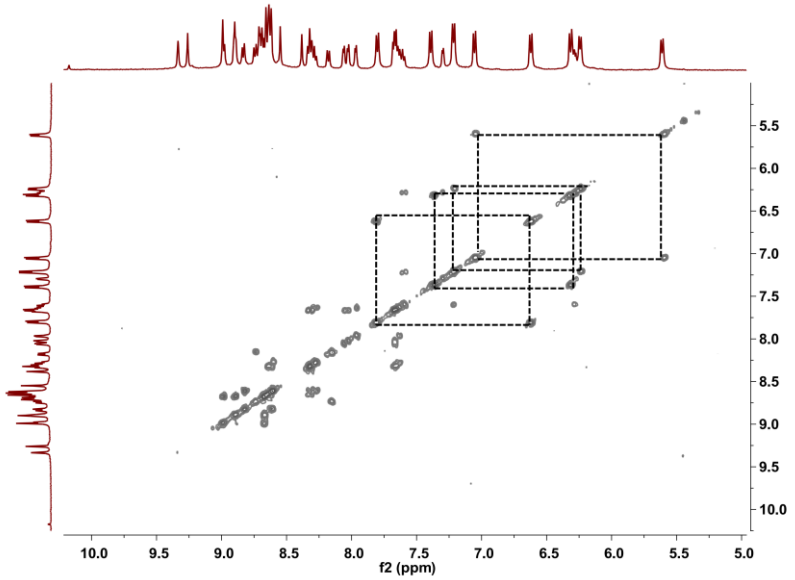

Figure S19. ^{1}H–^{1}H COSY spectrum of **Cat**-I $[Zn_8L_8][I]_7$ (400 MHz, CD_3CN, 298K).

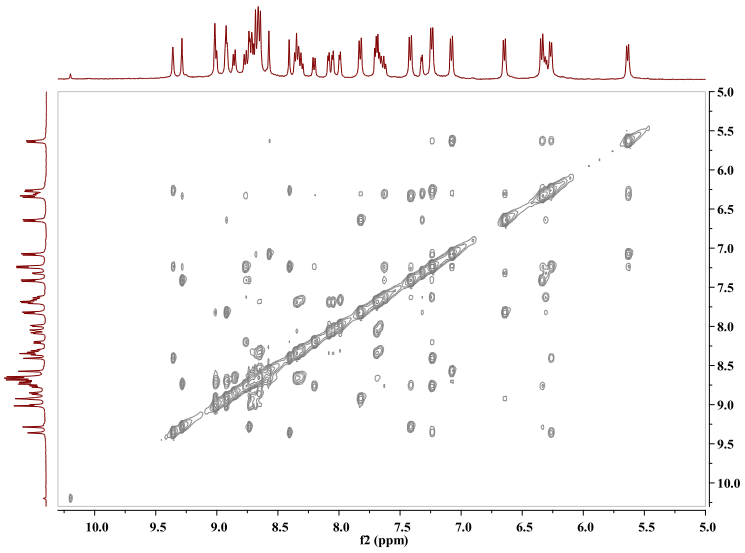

Figure S20. ^{1}H–^{1}H NOESY spectrum of **Cat**-I $[Zn_8L_8][I]_7$ (400 MHz, CD_3CN, 298K).

3. X-ray crystallography

Crystals of the interlocked **Cat-BF_4** suitable for X-ray diffraction were obtained by slow diffusion of diethyl ether into an acetonitrile solution of complex in a few days. Crystals of the interlocked **Cat-I/BF_4** suitable for X-ray diffraction were obtained by slow diffusion of diethyl ether into an acetonitrile solution of complex **Cat**-I with the presence of 10 equivalent of BF_4^- in a few days. The crystals were very susceptible to loss of solvent. Despite rapid handling times and a low temperature collection, the quality of data was less than ideal.

X-Ray intensity data were measured on a Bruker SMART APEX CCD-based diffractometer (Mo–Kα radiation, λ = 0.71073 Å) using the SMART and SAINT programs.[3,4] The crystal data was solved by direct methods and further refined by full-matrix least-squares refinements on F^2 using the SHELXL-97 software and an absorption correction was performed using the SADABS program.[5] Non-H atoms were refined with anisotropic displacement parameters. The hydrogen atoms within the ligand backbones and the solvent CH_3CN molecules were fixed geometrically at calculated distances and allowed to ride on the parent non-hydrogen atoms. The highly disordered state of the incorporated molecule solvents meant that lots of them could not be located, and hence in the final refinement, the electron density within the cages was treated with the SQUEEZE routine in the PLATON program package.[6]

For the refinement of **Cat-BF_4,** several atoms on some pyridine rings of the ligands were disordered into two parts, with the site occupancy factors (s.o.f.) of each parts being fixed as 0.5, respectively**.** Several fluoride atoms in BF_4^- anions were disordered into two parts with the s.o.f. of each parts being refined with fixed value. Except the disordered parts and the partially occupied solvent molecules and partially occupied anions, the other non-hydrogen atoms were refined

anisotropically. Hydrogen atoms within the ligand backbones were fixed geometrically at calculated distances and allowed to ride on the parent non-hydrogen atoms. Bond distance of some pyridine and benzene rings, as well as several BF_4^- anions were restrained as idealized values. Thermal parameters on adjacent atoms of the ligand backbone and the BF_4^- groups were restrained to be similar. The SQUEEZE subroutine in PLATON was used.

For the refinement of **Cat**-I/BF_4, except half occupied several iodine ions sited at the central of the catenane, other iodine ions share the site with boron atoms of the BF_4^- anions, with the s.o.f. of each parts being fixed in suitable value. Some pyridine rings of the ligands were disordered into two parts, with the site occupancy factors (s.o.f.) of each parts being fixed as fixed value, respectively**.** Several fluoride atoms in a partially occupied BF_4^- anion were disordered into two parts with the s.o.f. of each parts being refined with fixed value, respectively. Except the disordered parts and the partially occupied solvent molecules and partially occupied anions, the other non-hydrogen atoms were refined anisotropically. Hydrogen atoms within the ligand backbones were fixed geometrically at calculated distances and allowed to ride on the parent non-hydrogen atoms. Bond distance of some pyridine and benzene rings, as well as several BF_4^- anions were restrained as idealized values. Thermal parameters on adjacent atoms of the disordered parts of the ligand backbone and the particularly occupied BF_4^- groups were restrained to be similar. The SQUEEZE subroutine in PLATON was used.

Table S1. Crystal data and structure refinements.

Compounds	**Cat-BF_4**	**Cat-I/BF_4**
CCDC	**1515722**	**1515723**
Empirical formula	$Zn_4C_{204}H_{158}N_{40}O_7B_8F_{32}$	$Zn_4C_{206}H_{163}N_{41}O_8B_{3.5}I_{4.5}F_{14}$
Formula weight	4237.66	4477.14
T/K	100(2)	150(2)
Crystal system	Monoclinic	Monoclinic
Space group	*C2/c*	*C2/c*
a/Å	47.6161(17)	47.061(2)
b/Å	31.7486(11)	32.0425(14)
c/Å	56.289(2)	55.568(3)
α/°	90.00	90
β/°	111.3046(16)	110.4064(10)
γ/°	90.00	90
V/Å^3	79279(5)	78535(7)
Z	8	8
D_{calc}/Mg m^{-3}	0.712	0.757
μ/mm^{-1}	0.289	0.637
F(000)	17376	18016
R_{int}	0.1629	0.1617
Data/parameters	69557/2723	68982/2704
GOF	0.959	0.967
R [$I > 2\sigma(I)$][a]	R_1 = 0.0985, wR_2 = 0.1935	R_1 = 0.0885, wR_2 = 0.2190
R indices (all data)	R_1 = 0.3793, wR_2 = 0.2896	R_1 = 0.2945, wR_2 = 0.2659
$\Delta\rho_{max,min}$/eÅ^{-3}	0.449/-0.241	0.680/-0.555

[a] $R_1 = \Sigma||F_o| - |F_c||/\Sigma|F_o|$; [b] $wR_2 = \Sigma[w(F_o^2 - F_c^2)^2]/\Sigma[w(F_o^2)^2]^{1/2}$

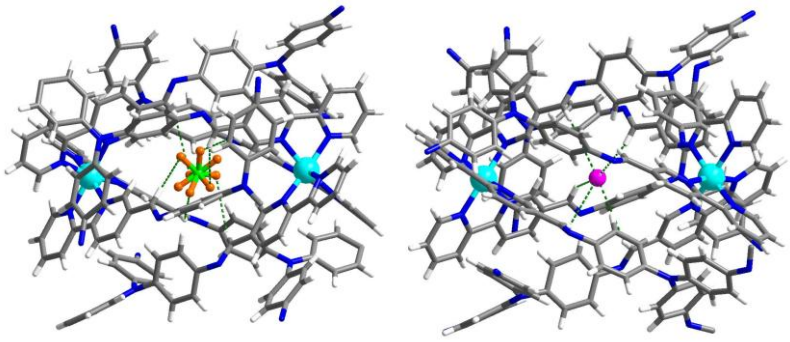

Figure S21. Enriched C-H・・・F interactions (green lines) in **Cat-BF_4** and C-H・・・I interactions (green lines) in **Cat-I/BF_4**.

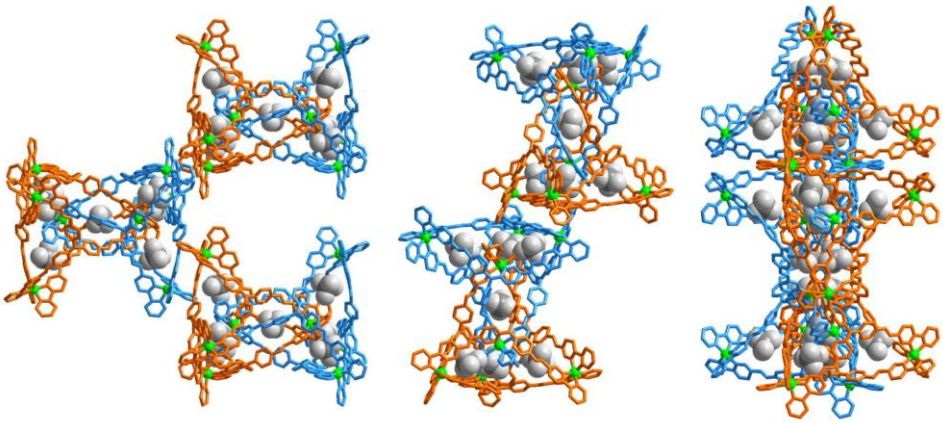

Figure S22. Packing of the interlocked cages in **Cat-BF_4** along a (left), b (middle) and c (right) axis.

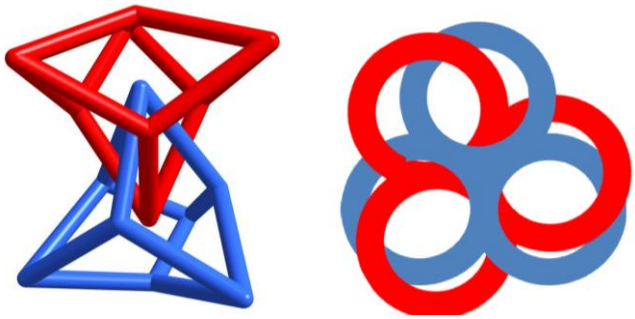

Figure S23. Schematic representation emphasizing the helical structure of interlocked dimers and the topology of the triply interlocked 3-torus dimer along the C_3 axis.

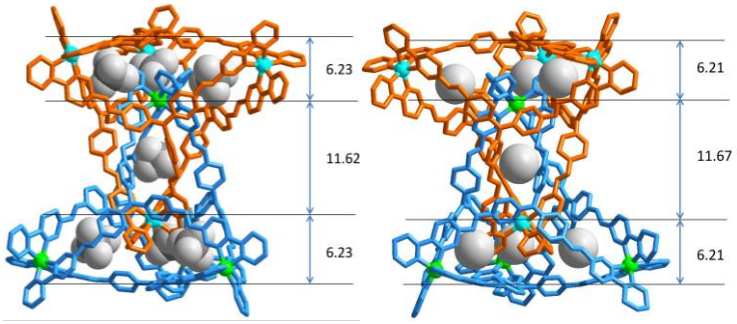

Figure S24. X-ray crystal structures of interlocked cage of (left) **Cat**-BF_4 and (right) **Cat**-I/BF_4 (the [7I⊂Zn_8L_8] species). The Zn−Zn distances of the nearest center are similar although in presence of different ions.

Table S2. Selected bond lengths and angles for **Cat**-BF_4 and **Cat**-I/BF_4.

Cat-BF_4			**Cat**-I/BF_4		
Atom	Atom	Length/Å	Atom	Atom	Length/Å
Zn(1)	N(2)	2.124(6)	Zn(1)	N(2)	2.113(5)
Zn(1)	N(1)	2.135(5)	Zn(1)	N(21)	2.129(5)
Zn(1)	N(11)	2.140(5)	Zn(1)	N(11)	2.131(5)
Zn(1)	N(12)	2.146(5)	Zn(1)	N(12)	2.138(5)
Zn(1)	N(31)	2.160(5)	Zn(1)	N(1)	2.149(6)
Zn(1)	N(32)	2.175(4)	Zn(1)	N(22)	2.156(6)
Zn(2)	N(21)	2.119(5)	Zn(2)	N(34)	2.068(6)
Zn(2)	N(17)	2.158(5)	Zn(2)	N(27)	2.101(7)
Zn(2)	N(35)	2.161(6)	Zn(2)	N(35)	2.144(5)
Zn(2)	N(22)	2.174(5)	Zn(2)	N(4)	2.152(6)
Zn(2)	N(34)	2.216(6)	Zn(2)	N(28)	2.173(10)
Zn(2)	N(18)	2.222(6)	Zn(2)	N(5)	2.348(13)
Zn(3)	N(7)	2.087(7)	Zn(3)	N(14)	2.061(8)
Zn(3)	N(27)	2.110(6)	Zn(3)	N(8)	2.111(6)
Zn(3)	N(8)	2.128(6)	Zn(3)	N(37)	2.140(6)
Zn(3)	N(37)	2.150(6)	Zn(3)	N(38)	2.163(5)
Zn(3)	N(38)	2.175(5)	Zn(3)	N(7)	2.167(5)
Zn(3)	N(28)	2.178(4)	Zn(3)	N(15)	2.172(5)
Zn(4)	N(15)	2.031(7)	Zn(4)	N(31)	2.089(7)
Zn(4)	N(14)	2.048(7)	Zn(4)	N(17)	2.092(6)
Zn(4)	N(4)	2.134(7)	Zn(4)	N(24)	2.129(8)
Zn(4)	N(24)	2.178(8)	Zn(4)	N(18)	2.134(6)
Zn(4)	N(25)	2.191(5)	Zn(4)	N(25)	2.155(5)
Zn(4)	N(5)	2.218(7)	Zn(4)	N(32)	2.158(6)

Atom	Atom	Atom	Angle/ °	Atom	Atom	Atom	Angle/ °
N(2)	Zn(1)	N(1)	75.8(2)	N(2)	Zn(1)	N(21)	93.7(2)
N(2)	Zn(1)	N(11)	94.8(2)	N(2)	Zn(1)	N(11)	169.2(2)
N(1)	Zn(1)	N(11)	94.9(2)	N(21)	Zn(1)	N(11)	93.5(2)
N(2)	Zn(1)	N(12)	96.8(2)	N(2)	Zn(1)	N(12)	96.2(2)
N(1)	Zn(1)	N(12)	167.7(2)	N(21)	Zn(1)	N(12)	168.2(2)
N(11)	Zn(1)	N(12)	75.8(2)	N(11)	Zn(1)	N(12)	77.7(2)
N(2)	Zn(1)	N(31)	166.7(2)	N(2)	Zn(1)	N(1)	77.0(2)
N(1)	Zn(1)	N(31)	94.0(2)	N(21)	Zn(1)	N(1)	93.2(2)
N(11)	Zn(1)	N(31)	94.5(2)	N(11)	Zn(1)	N(1)	94.6(2)
N(12)	Zn(1)	N(31)	94.6(2)	N(12)	Zn(1)	N(1)	95.3(2)
N(2)	Zn(1)	N(32)	96.2(2)	N(2)	Zn(1)	N(22)	94.5(2)
N(1)	Zn(1)	N(32)	93.9(3)	N(21)	Zn(1)	N(22)	76.0(2)
N(11)	Zn(1)	N(32)	167.3(2)	N(11)	Zn(1)	N(22)	95.1(2)
N(12)	Zn(1)	N(32)	96.7(2)	N(12)	Zn(1)	N(22)	96.8(2)
N(31)	Zn(1)	N(32)	75.7(2)	N(1)	Zn(1)	N(22)	165.9(2)
N(21)	Zn(2)	N(17)	97.3(2)	N(34)	Zn(2)	N(27)	98.5(3)
N(21)	Zn(2)	N(35)	169.9(2)	N(34)	Zn(2)	N(35)	76.7(2)
N(17)	Zn(2)	N(35)	92.0(2)	N(27)	Zn(2)	N(35)	96.3(2)
N(21)	Zn(2)	N(22)	75.8(2)	N(34)	Zn(2)	N(4)	94.5(3)
N(17)	Zn(2)	N(22)	166.8(2)	N(27)	Zn(2)	N(4)	95.7(3)
N(35)	Zn(2)	N(22)	95.7(2)	N(35)	Zn(2)	N(4)	166.1(3)
N(21)	Zn(2)	N(34)	97.9(2)	N(34)	Zn(2)	N(28)	169.2(3)
N(17)	Zn(2)	N(34)	95.2(2)	N(27)	Zn(2)	N(28)	74.7(3)
N(35)	Zn(2)	N(34)	77.5(2)	N(35)	Zn(2)	N(28)	95.4(3)
N(22)	Zn(2)	N(34)	96.9(2)	N(4)	Zn(2)	N(28)	94.5(4)
N(21)	Zn(2)	N(18)	92.9(2)	N(34)	Zn(2)	N(5)	92.4(5)
N(17)	Zn(2)	N(18)	77.6(2)	N(27)	Zn(2)	N(5)	164.6(4)
N(35)	Zn(2)	N(18)	92.8(2)	N(35)	Zn(2)	N(5)	96.7(3)
N(22)	Zn(2)	N(18)	91.4(2)	N(4)	Zn(2)	N(5)	72.6(3)
N(34)	Zn(2)	N(18)	167.7(2)	N(28)	Zn(2)	N(5)	95.9(5)

4. ESI-MS analysis

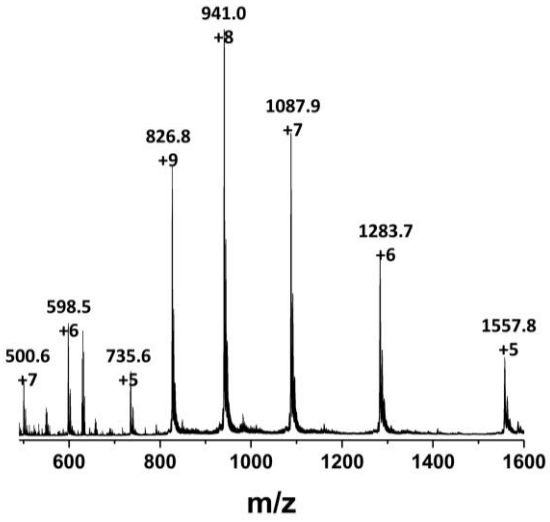

Figure S25. ESI-MS of **Cat-BF_4**, showing the formation of interlocked cage and the presence of unconverted individual cage.

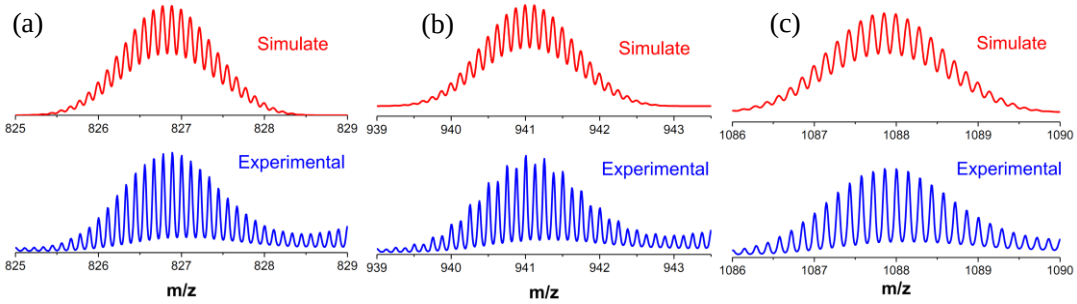

Figure S26. HRMS analysis of **Cat-BF_4**, showing the theoretical isotope model (top) and the observed data (bottom) for $[Zn_8L_8(BF_4)_7]^{9+}$(a), $[Zn_8L_8(BF_4)_8]^{8+}$(b) and $[Zn_8L_8(BF_4)_9]^{7+}$(c).

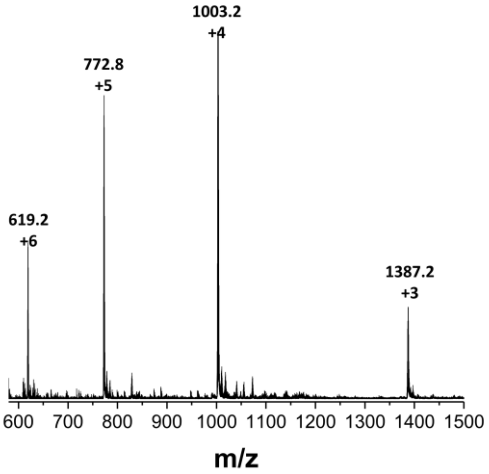

Figure S27. ESI-MS of **Tet**-1, showing the formation of individual cage

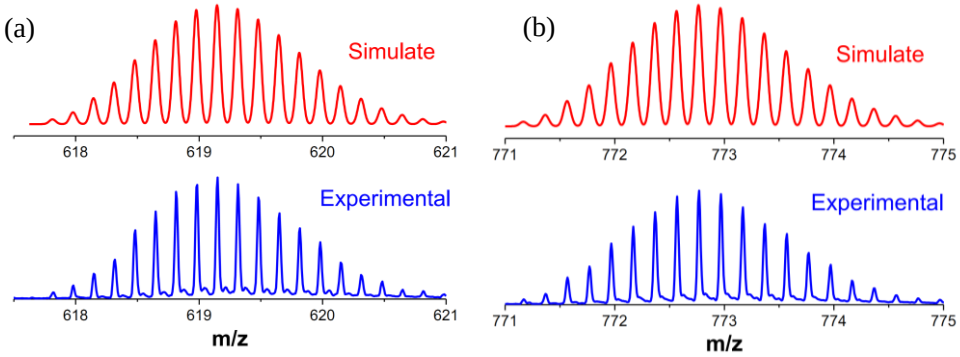

Figure S28. HRMS analysis of **Tet**-1, showing the theoretical isotope model (top) and the observed data (bottom) for $[Zn_4L_4(CF_3SO_3)_2]^{6+}$(a) and $[Zn_4L_4(CF_3SO_3)_3]^{5+}$(b).

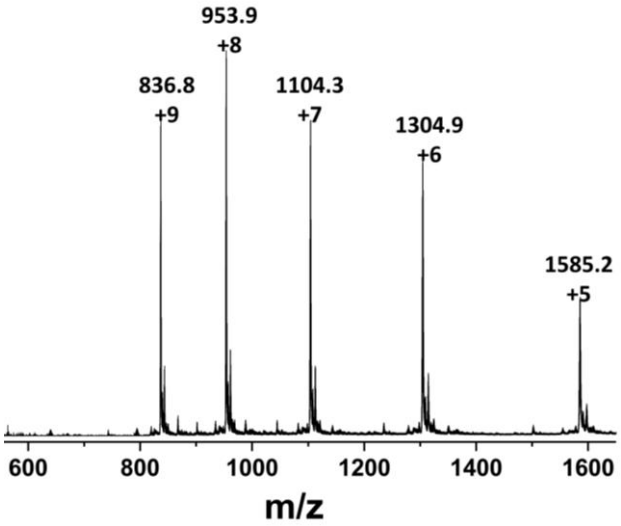

Figure S29. ESI-MS of **Cat-ClO_4**, showing the formation of interlocked cage, and seven ClO_4^- anions are tightly trapped in **Cat-ClO_4**.

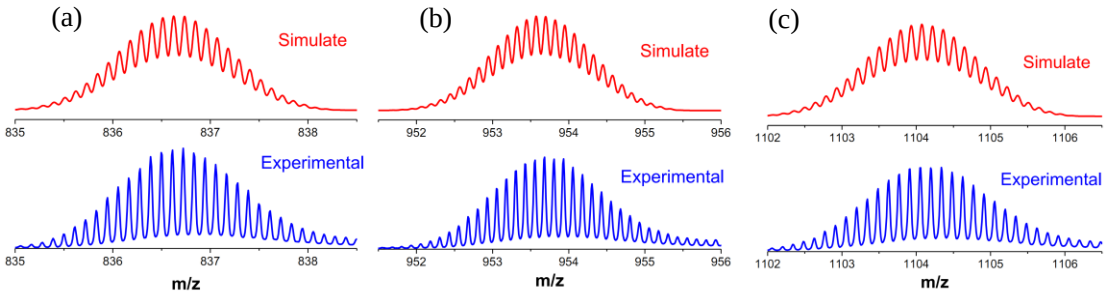

Figure S30. HRMS analysis of **Cat-ClO$_4$**, showing the theoretical isotope model (top) and the observed data (bottom) for $[Zn_8L_8(ClO_4)_7]^{9+}$(a) and $[Zn_8L_8(ClO_4)_8]^{8+}$(b), $[Zn_8L_8(ClO_4)_9]^{7+}$(c).

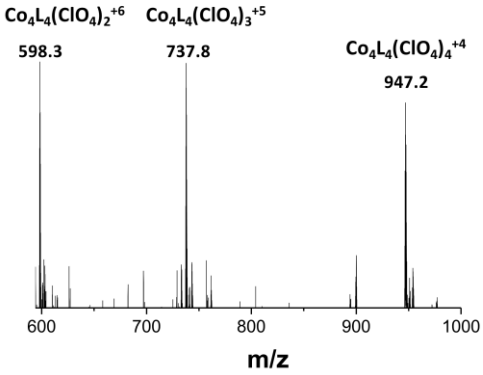

Figure S31. ESI-MS of Tet-Co **[Co$_4$L$_4$][ClO$_4$]**, showing the individual tetrahedron cage.

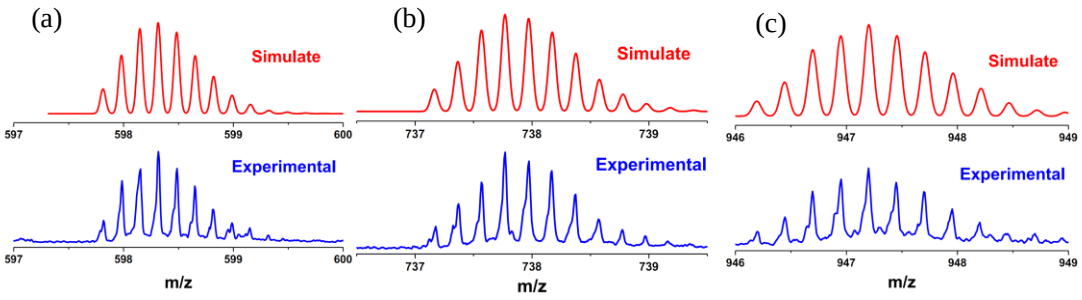

Figure S32. HRMS analysis of Tet-Co [Co$_4$L$_4$], showing the theoretical isotope model (top) and the observed data (bottom) for $[Co_4L_4(ClO_4)_2]^{6+}$(a) and $[Co_4L_4(ClO_4)_3]^{5+}$(b), $[Co_4L_4(ClO_4)_4]^{4+}$(c).

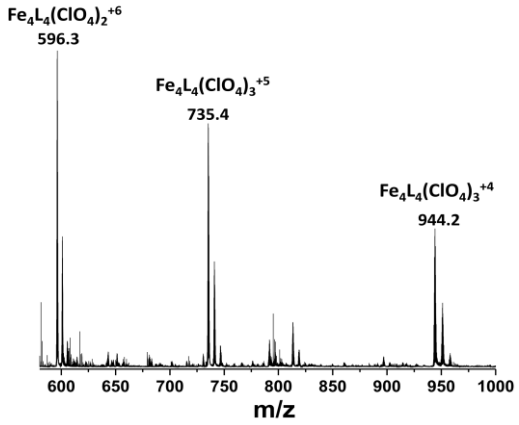

Figure S33. ESI-MS of Tet-3 [**Fe_4L_4][(ClO_4)]**, showing the individual cage.

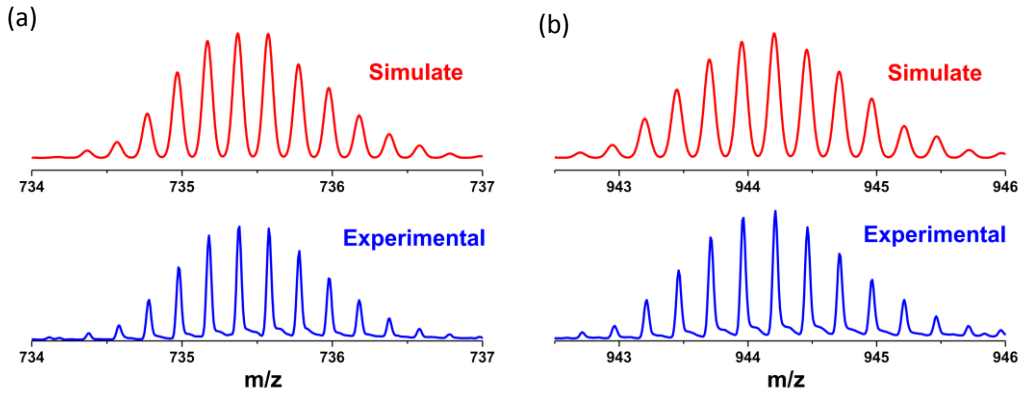

Figure S34. HRMS analysis of Tet-Fe [Fe_4L_4], showing the theoretical isotope model (top) and the observed data (bottom) for $[Fe_4L_4(ClO_4)_3]^{5+}$(a) and $[Fe_4L_4(ClO_4)_4]^{4+}$(b).

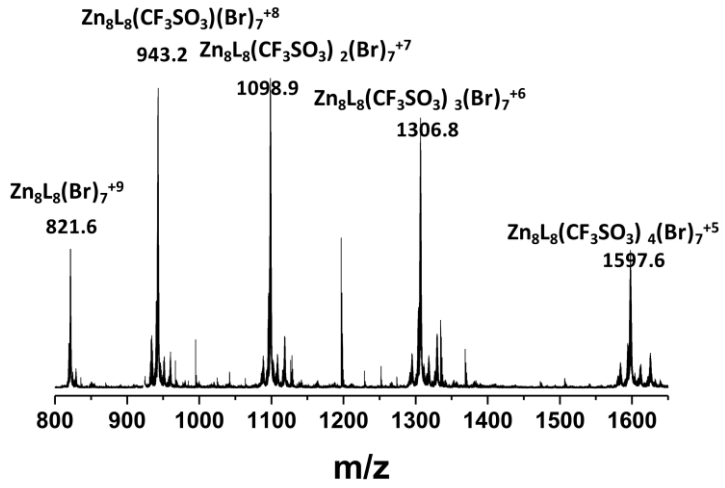

Figure S35. ESI-MS of **Cat**-Br, showing the formation of interlocked cage, and seven Br^- anions are tightly trapped in **Cat**-Br.

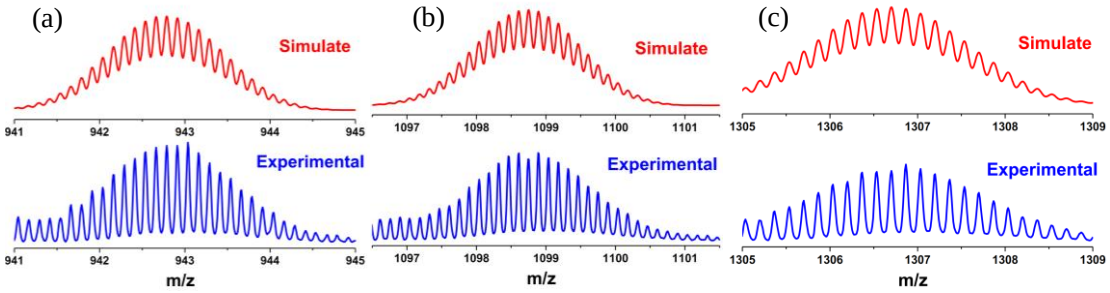

Figure S36. HRMS analysis of **Cat**-Br, showing the theoretical isotope model (top) and the observed data (bottom) for $[Zn_8L_8Br_7(CF_3SO_3)]^{8+}$(a), $[Zn_8L_8Br_7(CF_3SO_3)_2]^{7+}$(b), and $[Zn_8L_8Br_7(CF_3SO_3)_3]^{6+}$(c).

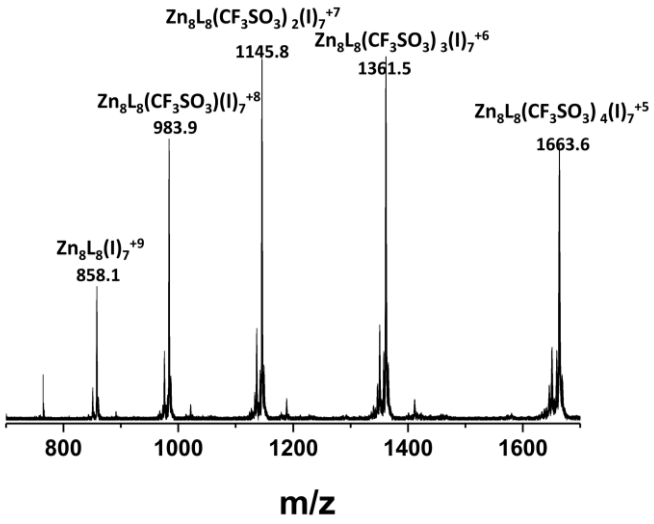

Figure S37. ESI-MS of **Cat**-I, showing the formation of interlocked cage, and seven I^- are tightly trapped in **Cat**-I.

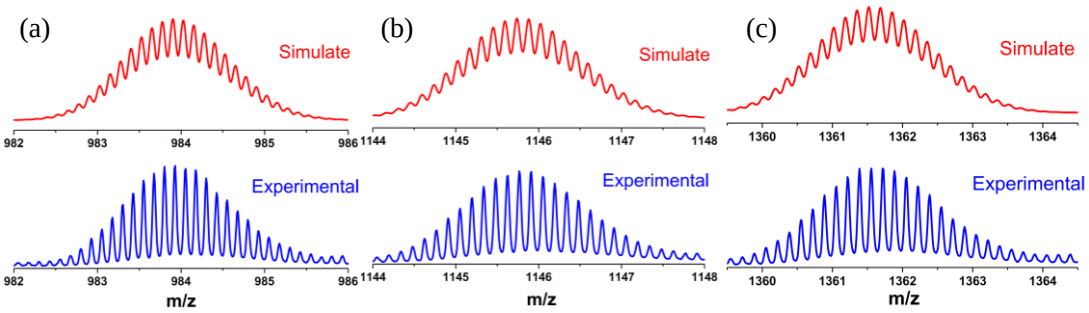

Figure S38. HRMS analysis of **Cat**-I, showing the theoretical isotope model (top) and the observed data (bottom) $[Zn_8L_8I_7(CF_3SO_3)]^{8+}$(a), $[Zn_8L_8I_7(CF_3SO_3)_2]^{7+}$(b), and $[Zn_8L_8I_7(CF_3SO_3)_3]^{6+}$(c).

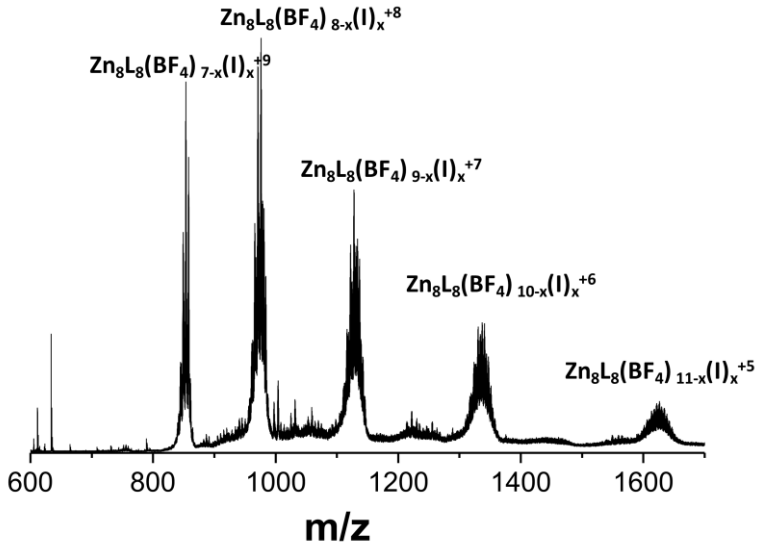

Figure S39. ESI mass spectrum of the **Cat**-I/BF_4 mixture: **Cat-I** with the addition of 10 equiv. Bu_4NBF_4, showing several I^- or BF_4^- anions random encapsulated in the cavity of **Cat**-I/BF_4.

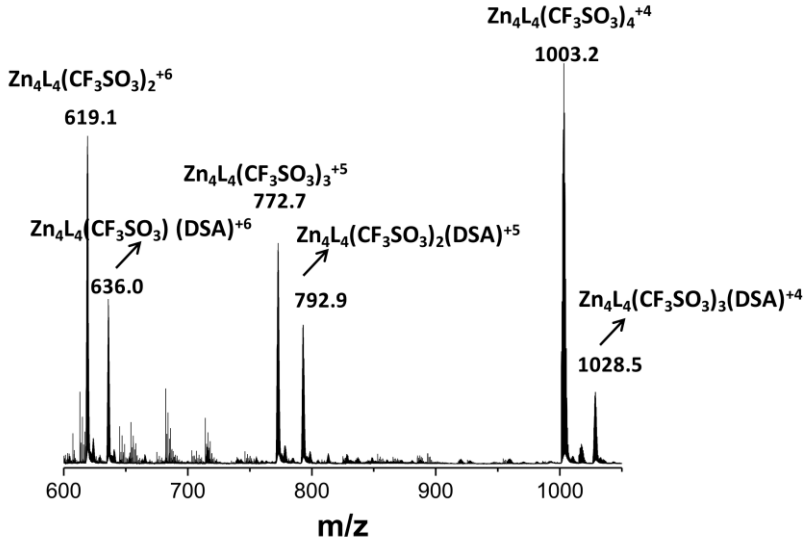

Figure S40. ESI mass spectrum of [**DSA⊂Tet**-1], showing one molecular dansyl acid(**DSA**) encapsulated in the **Tet**-1.

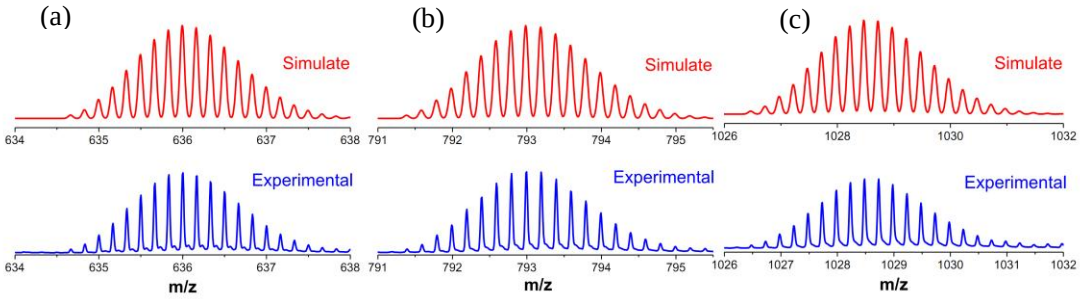

Figure S41. HRMS analysis of [**DSA**⊂**Tet**-1], showing the theoretical isotope model (top) and the observed data (bottom) $[Zn_4L_4(\mathbf{DSA})(CF_3SO_3)]^{6+}$(a), $[Zn_4L_4(\mathbf{DSA})(CF_3SO_3)_2]^{5+}$(b), and $[Zn_4L_4(\mathbf{DSA})(CF_3SO_3)_3]^{4+}$(c).

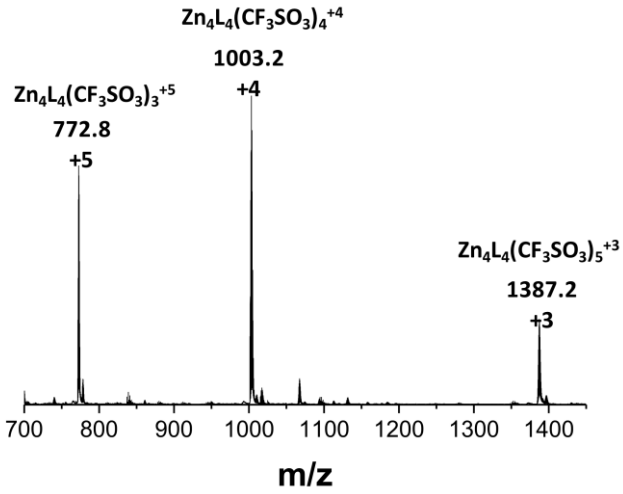

Figure S42. ESI mass spectrum of interlocked cage **Cat**-I with the addition of 10 equiv of $AgCF_3SO_3$, which were assigned to the discrete cage **Tet**-1.

5. NMR titrations

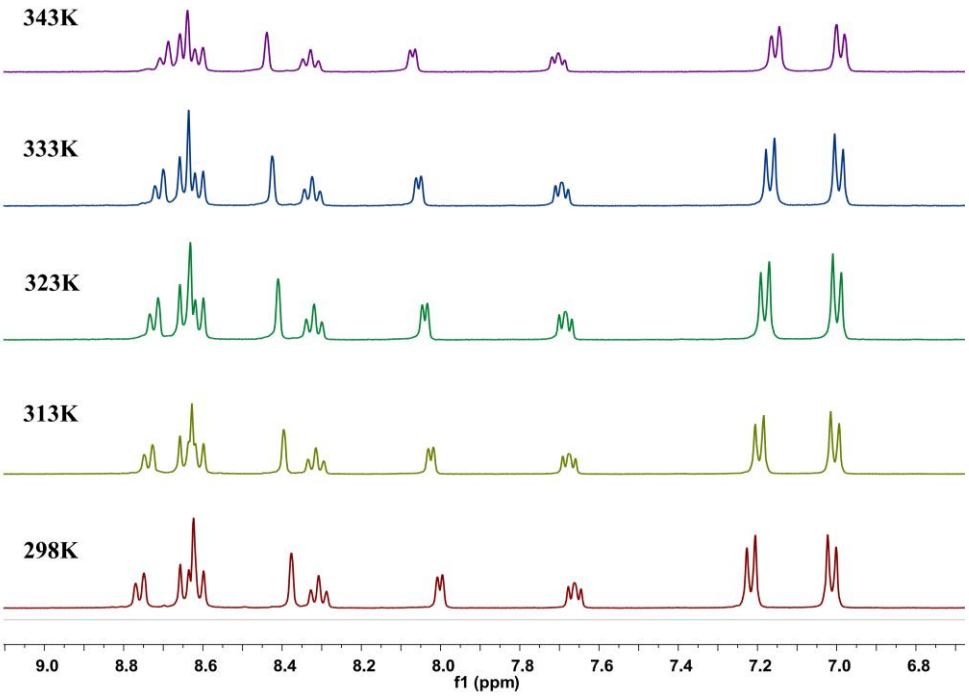

Figure S43. Variable-temperature ^{1}H NMR spectra (400 MHz, CD_3CN) of **Tet**-1 at different temperature. No interlocked peaks are observed shown the high thermostability of **Tet**-1.

5.1 Transformation Experiments of Tetrahedron to Catenane

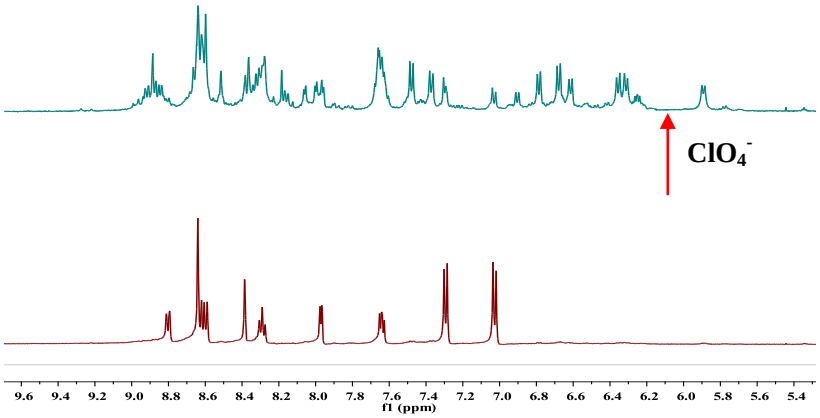

Figure S44. Variation of the ^{1}H NMR spectrum (400 MHz, 298 K) with the addition of 20 equiv of ClO_4^- to the solution of **Tet**-1 (2 mM) for several days. The formation of interlocked cage is confirmed by appearance of the new set of peaks.

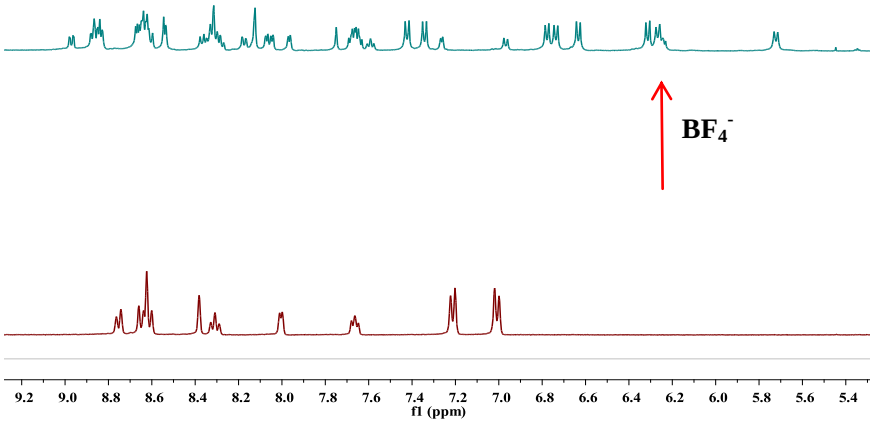

Figure S45. Variation of the ^{1}H NMR spectrum (400 MHz, 298 K) with the addition of 20 equiv of BF_4^- to the solution of **Tet**-1 (2 mM) for several days. The formation of interlocked cage is confirmed by appearance of the new set of peaks.

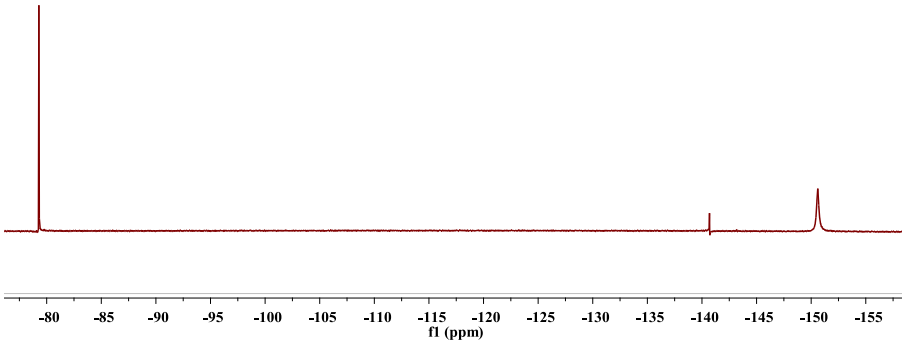

Figure S46. ^{19}F NMR spectrum (376 MHz, CD_3CN, 298 K) of **Tet**-1 in addition of 20 equiv of Bu_4NBF_4. δ(ppm)= -143.32 (encapsulated BF_4^-), -151.70 (broad signal, free BF_4^-), -79.28 (residual $CF_3SO_3^-$ of **Tet**-1).

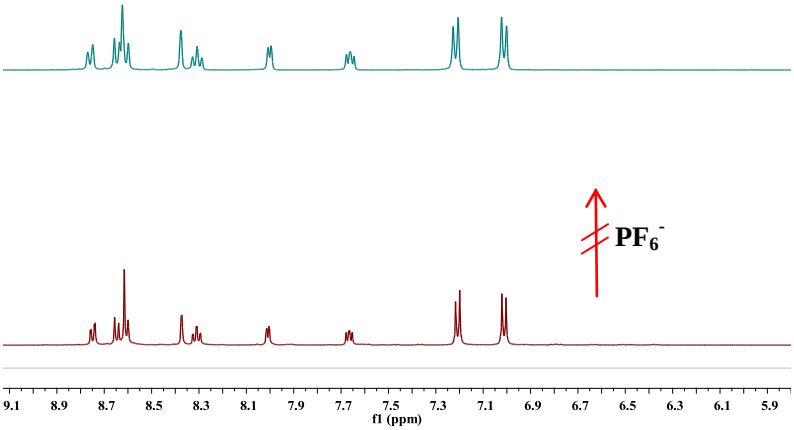

Figure S47. Variation of the ^1H NMR spectrum (400 MHz, 298 K) with the addition of 20 equiv of PF_6^- to the solution of **Tet**-1 (2 mM). No peak changes appeared indicated that the PF_6^- could not induce the formation of the interlocked structure.

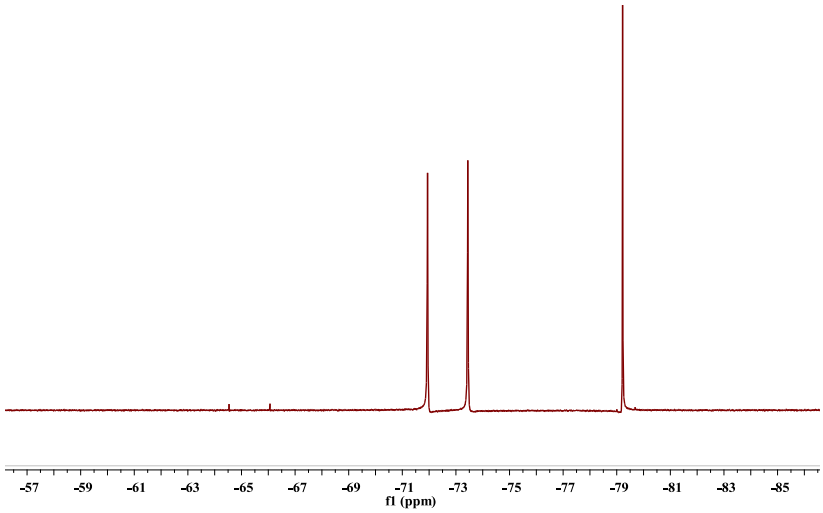

Figure S48. ^{19}F NMR spectrum (376 MHz, CD_3CN, 298 K) of **Tet**-1 in the presence of 20 equiv of Bu_4NPF_6. δ(ppm) = –71.94, –73.44 (PF_6^-), –79.28 (residual $CF_3SO_3^-$ of **Tet**-1).

5.2 General procedure for thermodynamics analysis for ClO_4^- and BF_4^- dependence

To a 10 mL flask, individual tetrahedron **Tet**-1(27.6 mg, 0.006 mmol, 1 equiv) was added as a solution in CD_3CN (3 mL). Then the internal standard 1,3,5-trimethoxybenzene(0.01 g, 0.06 mmol, 10 equiv) was added to the solution and the mixture was stirring for 5 min. The mixture was then taken out with 0.5mL solution for NMR spectrometer. Prior to the thermodynamics experiment, by microliter syringe the desired amount of Bu_4NClO_4 or Bu_4NBF_4 (0.5 M) was added as a solution in CD_3CN. The reaction mixture was standing at room temperature for 24 hour, and then the NMR spectrometer was recorded. The conversion of the dimerization reaction was calculated by the change of integral area of Ha in Tet-1 at 7.0 ppm based on the internal standard.

To calculate the rate constant, the following assumptions were made:

Equation of equilibrium: 2 **Tet**-1+ ClO_4^- ⇌ **Cat-ClO_4**

When n equiv anions added: C_0 nC_0

Equilibrium state: C_0-2xC_0 C_0- xC_0 xC_0

Then (x is the conversion) $K= xC_0/((C_0-2xC_0)^2 (C- xC_0))$

$$\log(n-x)+\log KC_0^2=\log(x/(1-2x)^2)$$

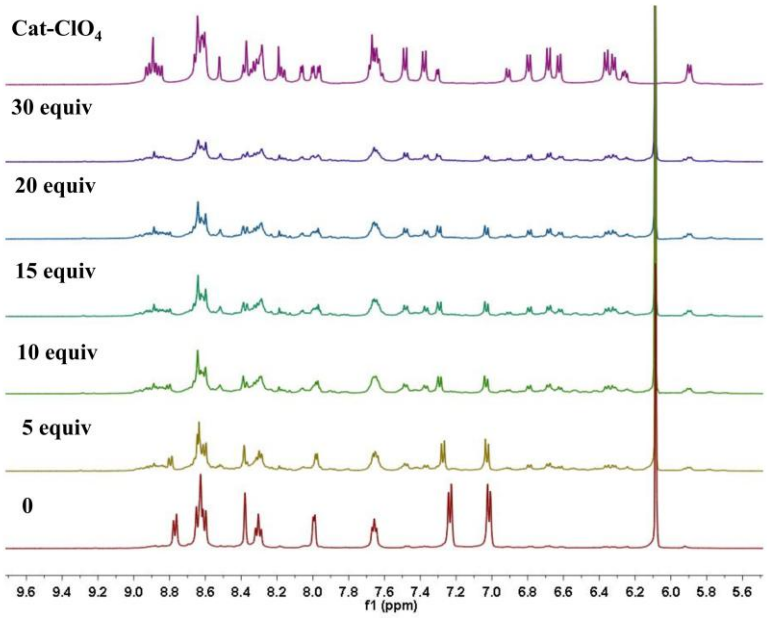

Figure S49. ^{1}H NMR spectra following the titration of Bu_4NClO_4 into **Tet**-1 (CD_3CN, 500 MHz) and equilibrium for 24h at 298K. The equivalents of ClO_4^- are indicated on the left side of the spectra. (* was label as the internal standard 1,3,5- trimethoxybenzene)

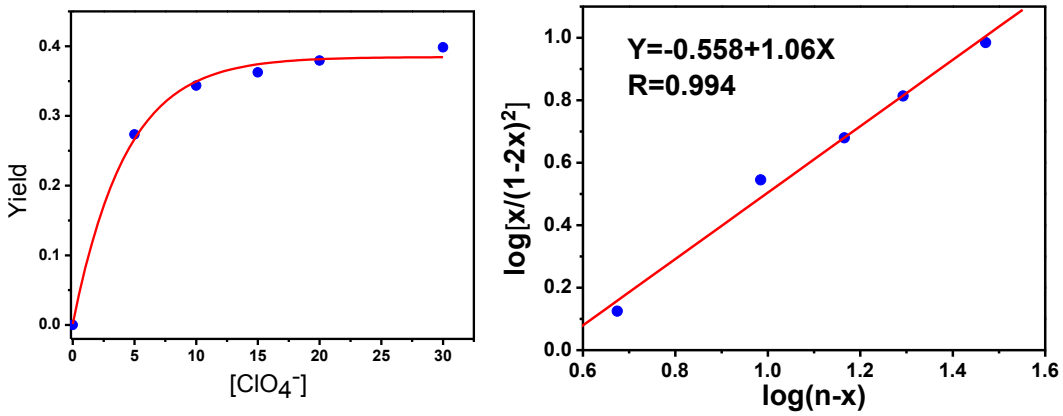

Figure S50. a) The fitting curve of the yield of **Cat-ClO$_4$** with different equiv of ClO_4^-, b) the linear fitting line of the transfer equilibrium, the slope of this line shows the thermodynamics equilibrium constant K.

With this assumption and the data extracted from Figure S50, the equilibrium constant at 298 K were determined as follows: $K = 10^{-0.558}/[C_0]^2 = 7\times10^4$ mol^{-2} L^{-2}. ΔG_{ClO4}=-27.6 kJ/mol.

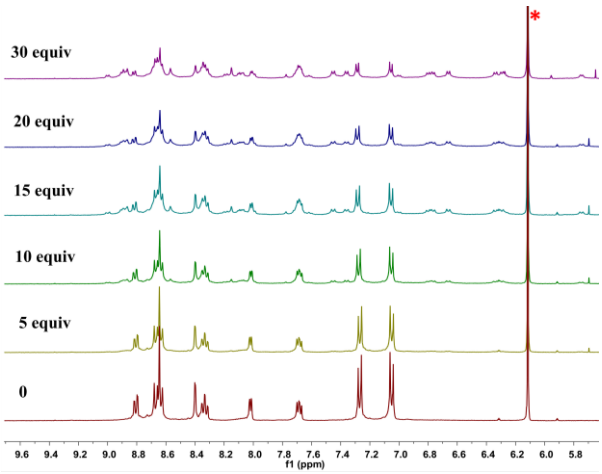

Figure S51. ^{1}H NMR spectra following the titration of Bu_4NBF_4 into **Tet**-1 (CD_3CN, 500 MHz) and equilibrium for 24h at 298K. The equivalents of BF_4^- are indicated on the left side of the spectra. (* was label as the internal standard 1,3,5- trimethoxybenzene).

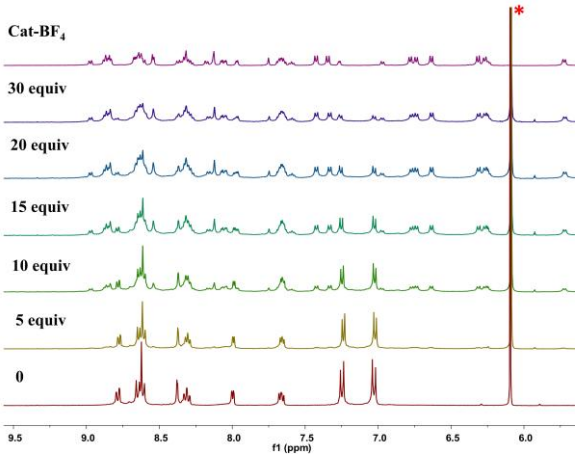

Figure S52. ^{1}H NMR spectra following the titration of Bu_4NBF_4 into **Tet**-1 (CD_3CN, 500 MHz) and equilibrium for 48h at 298K. The equivalents of BF_4^- are indicated on the left side of the spectra. (* was label as the internal standard 1,3,5- trimethoxybenzene).

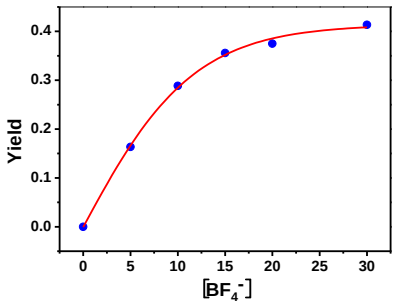

Figure S53. The fitting curve of the yield of **Cat-BF$_4$** with different equiv of BF_4^-.

6. Kinetics measurements for dimerization of cage **Tet**-1

The dimerization reaction involves at least two monomer cages, and probably encapsulation of ClO_4^- anions. To simplifying the process treatment, excess ClO_4^- anions are added to reach a saturated solution, thereof minimizing the influence of ClO_4^- anions on the reaction. To an NMR tube, individual tetrahedron **Tet**-1(4.6 mg, 2 mM, 1 equiv) was added as a solution in CD_3CN (0.5 mL). The internal standard 1,3,5-trimethoxybenzene (0.0016 g, 0.01 mmol) was added to the solution. The NMR tube was then fitted with a septum top, followed by the application of parafilm to seal the edges of the septum. Prior to the kinetics experiment, 20 equiv of Bu_4NClO_4 was added as a solution in CD_3CN. The reaction mixture was then placed into the prewarmed, tuned and shimmed NMR spectrometer at different temperature 313, 318, 323, 328 and 333 K. Then an automatic kinetics program was used to collect regular time points at 5 to 30 min intervals, depending on the rate of the reaction. The conversion of the dimerization reaction was calculated by the change of integral area of Ha in Tet-1 at 7.0 ppm based on the internal standard.

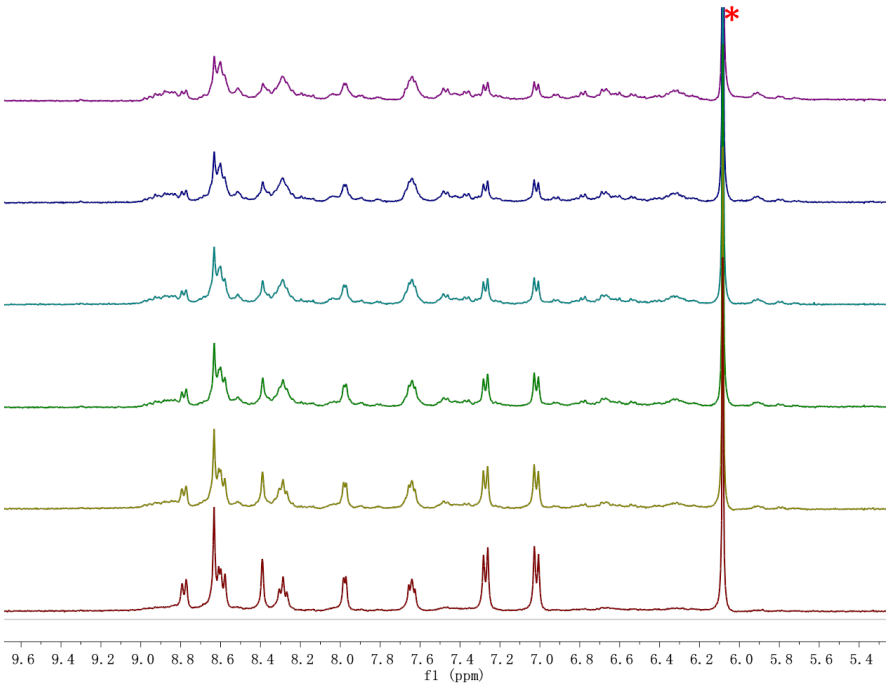

Figure S54. ^{1}H NMR spectrum (CD_3CN) of **Tet**-1 (2 mM) addition of 20 equiv of ClO_4^- maintained at **313K** with different time points of 30 min. (* label as the internal standard 1,3,5-trimethoxybenzene).

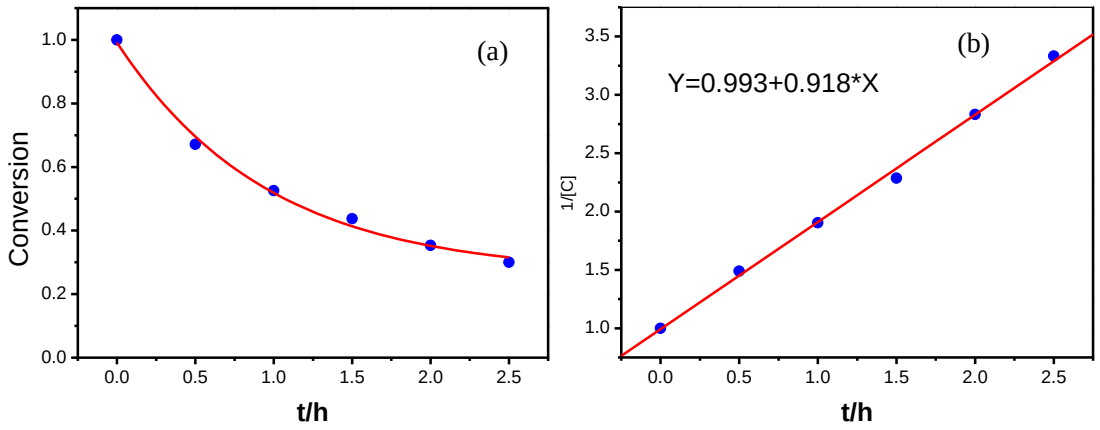

Figure S55. a) A representative kinetic trace of structure transfer process from **Tet**-1 to **Cat-ClO_4**; b) Kinetic plot Fitting used to determine a second-order rate constant for the reaction process at **313K**.

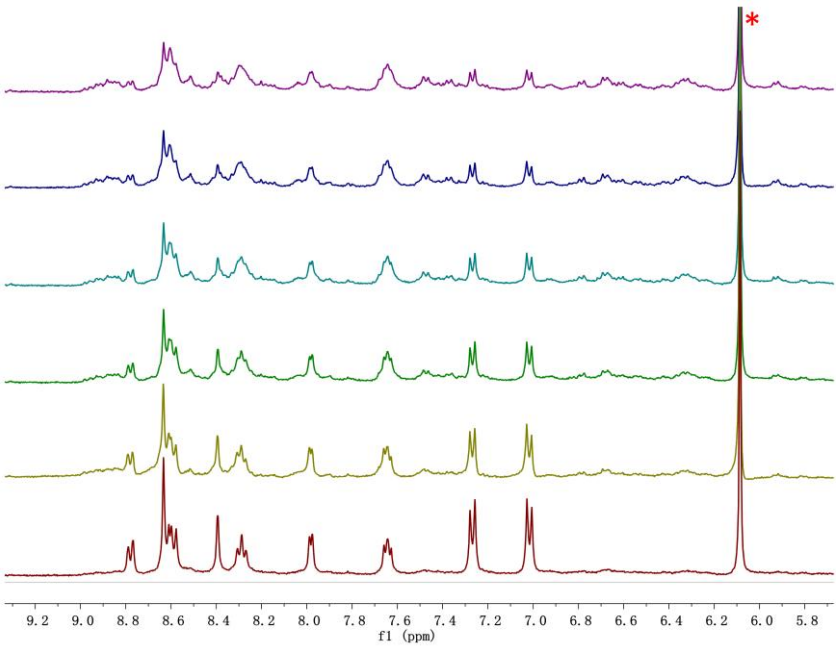

Figure S56. ^{1}H NMR spectrum (CD_3CN) of **Tet**-1 (2 mM) addition of 20 equiv of ClO_4^- maintained at **318K** with different time points of 20 min.

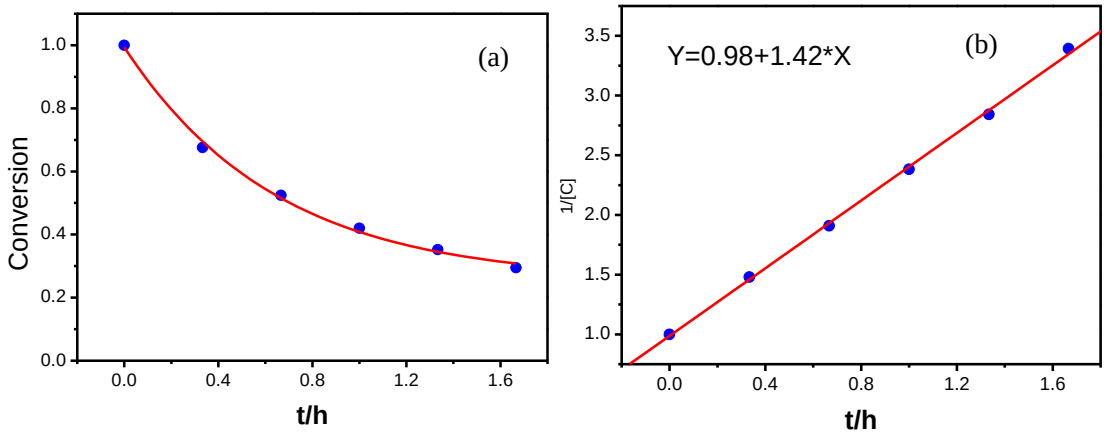

Figure S57. a) A representative kinetic trace of structure transfer process from **Tet**-1 to **Cat-ClO_4**; b) Kinetic plot fitting used to determine a second-order rate constant for the reaction process at **318K**.

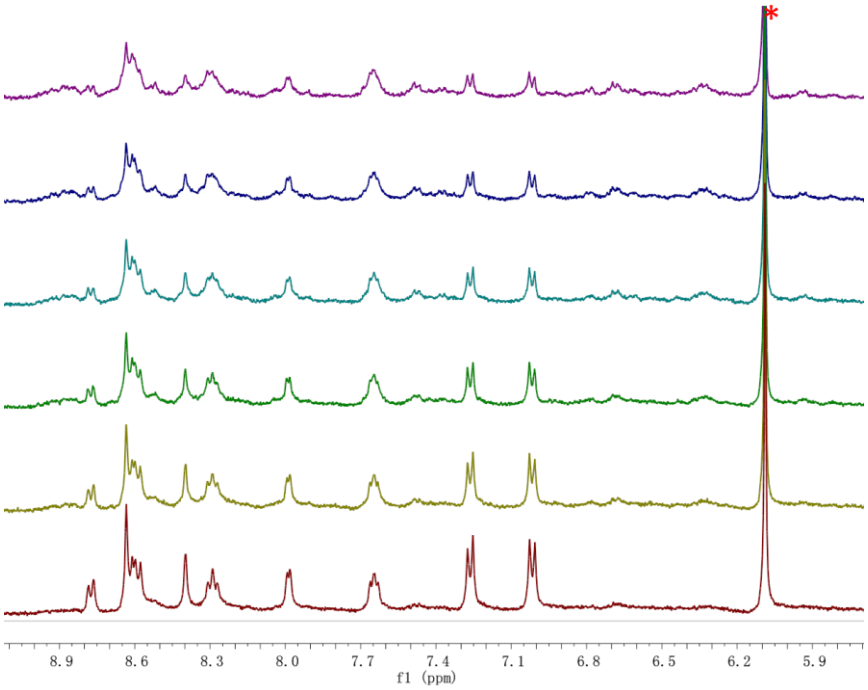

Figure S58. ^{1}H NMR spectrum (CD_3CN) of **Tet**-1 (2 mM) addition of 20 equiv of ClO_4^- maintained at **323K** with different time points of 10 min.

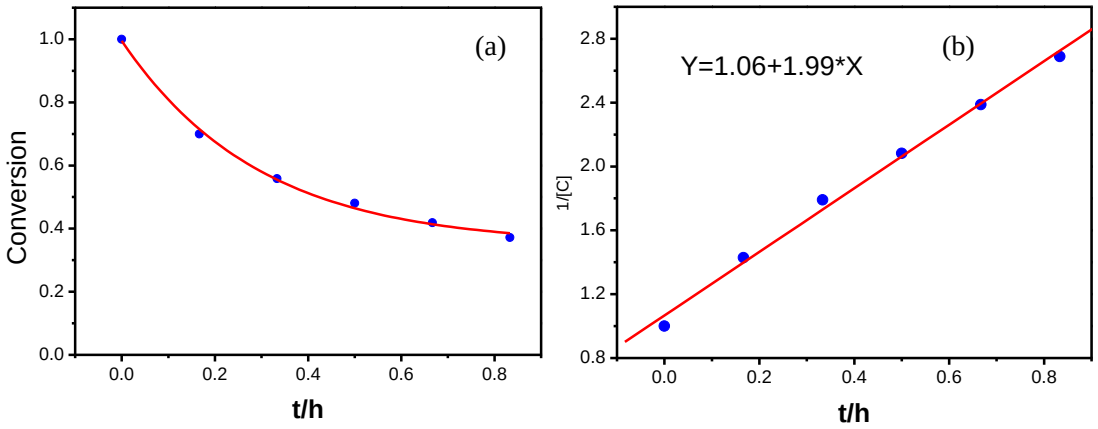

Figure S59. a) A representative kinetic trace of structure transfer process from **Tet**-1 to **Cat-ClO$_4$**; b) Kinetic plot Fitting used to determine a second-order rate constant for the reaction process at **323K**.

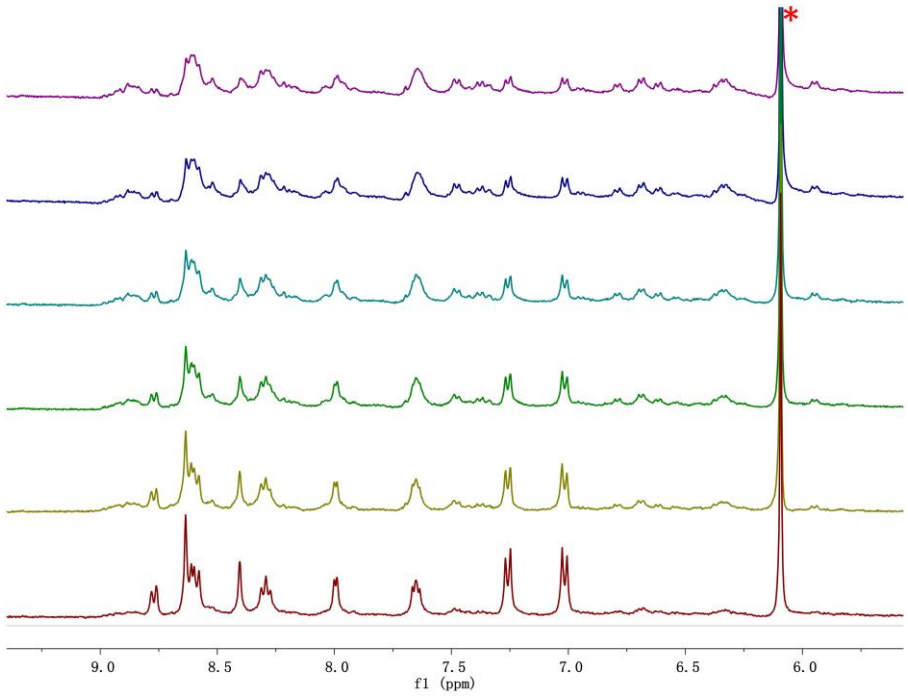

Figure S60. ^{1}H NMR spectrum (CD_3CN) of **Tet**-1 (2 mM) addition of 20 equiv of ClO_4^- maintained at **328K** with different time points of 10 min.

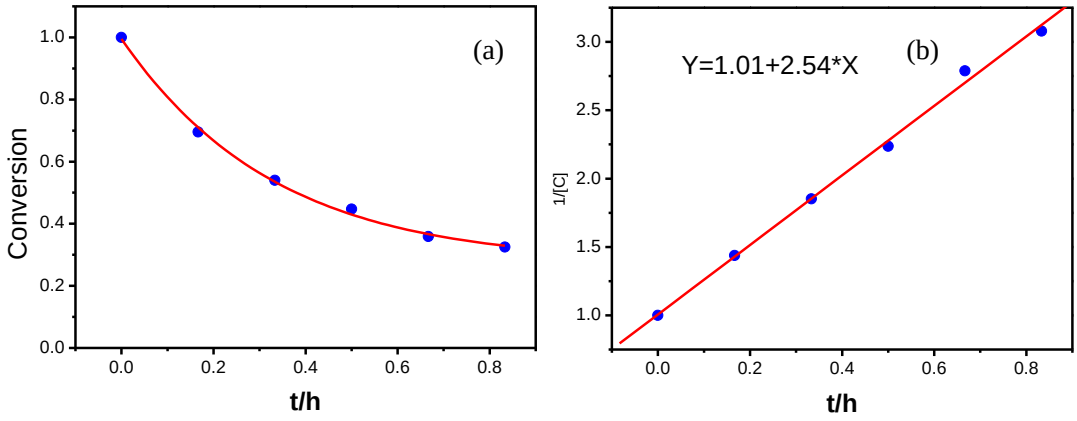

Figure S61. a) A representative kinetic trace of structure transfer process from **Tet**-1 to **Cat-ClO$_4$**; b) Kinetic plot Fitting used to determine a second-order rate constant for the reaction process at **328K**.

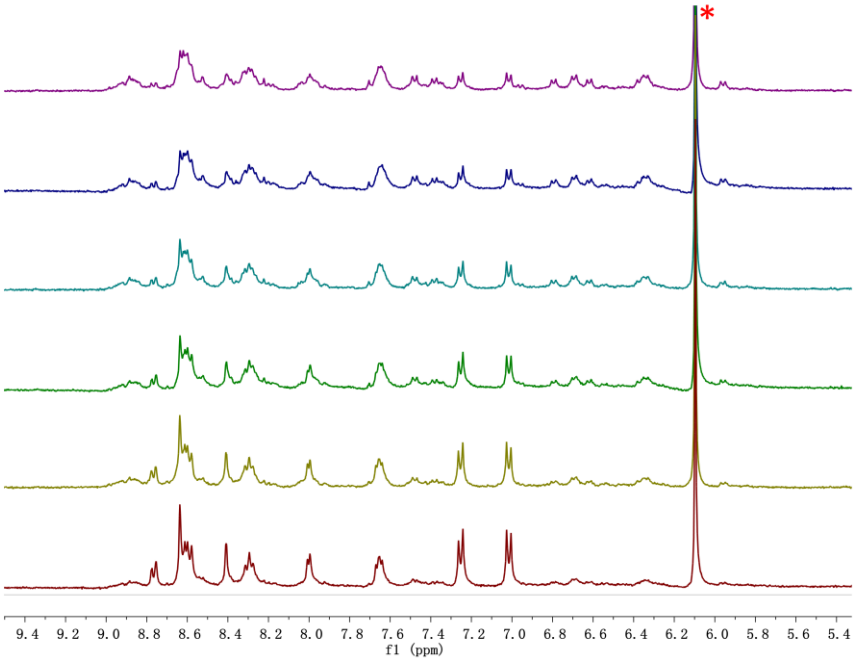

Figure S62. ^{1}H NMR spectrum (CD_3CN) of **Tet**-1 (2 mM) addition of 20 equiv of ClO_4^- maintained at **333K** with different time points of 5min.

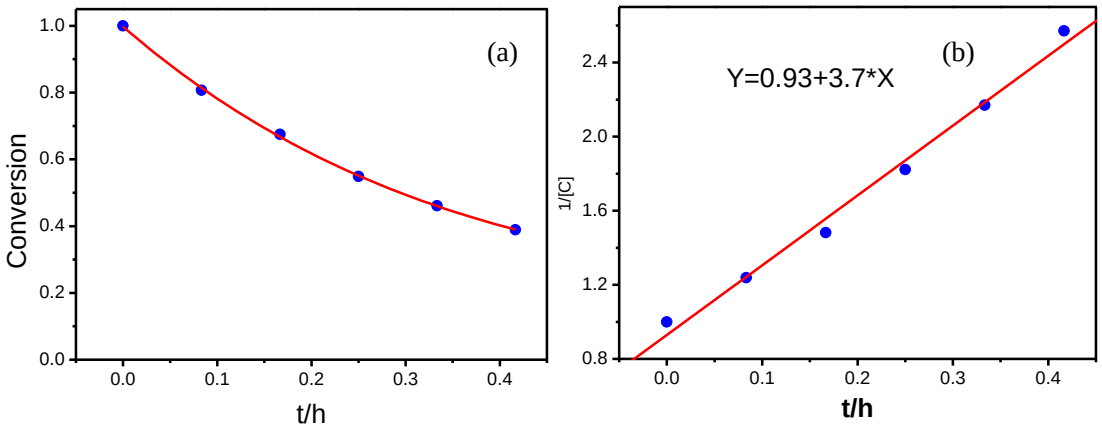

Figure S63. a) A representative kinetic trace of structure transfer process from **Tet**-1 to **Cat-ClO4**; b) Kinetic plot Fitting used to determine a second-order rate constant for the reaction process at **333K**.

Table S3. Second-order rate constants.

Temperature /K	Rate constant / $M^{-1}h^{-1}$	Rate constant / $M^{-1}s^{-1}$
313	454	0.126
318	698	0.194
323	994	0.276
328	1270	0.353
333	1879	0.522

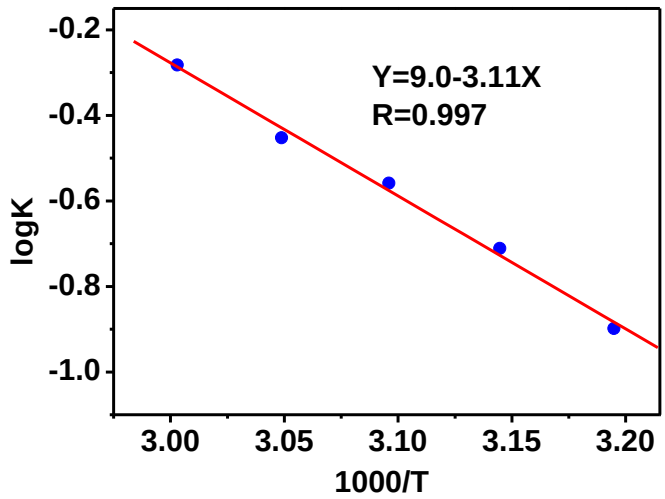

Figure S64. An Arrhenius plot measured activation energy based on temperature dependence of the structure transfer process. **Ea**/2.303R = 3.11, **Ea** = 59.5 kJ/mol.

7. The allosteric process with the titration of halide anions (Br^- and I^-)

General procedure

The interlocked catenane **Cat**-X were formed by titrating a solution of the halide (as their tetrabutyl ammonium salts in CD_3CN, 0.1 M) in steps of 1 eq. (10 μL) to 500 μL of a 2 mM solution of the **Tet**-1 in CD_3CN in an NMR tube. The NMR spectrum was recorded after each addition and the sample was mixed thoroughly before each measurement.

7.1 Titration of Tet-1 with NBu_4Br

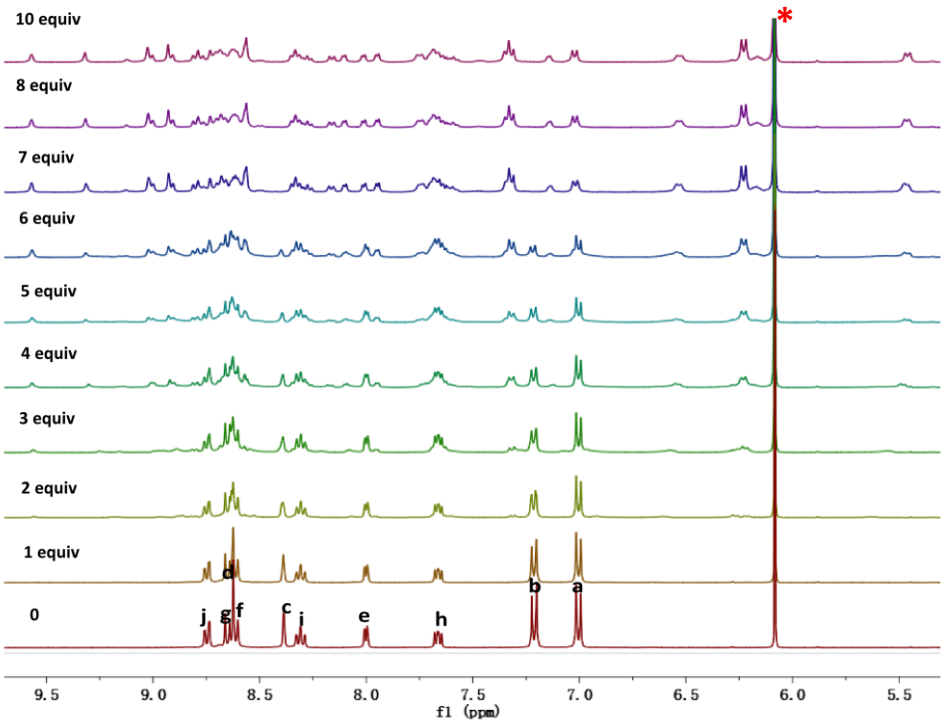

Figure S65. ^1H NMR spectra following the titration of Bu_4NBr into **Tet**-1 (CD_3CN, 400 MHz) and recorded immediately at 298K. The equivalents of Br^- are indicated on the left side of the spectra. (* was label as the internal standard 1,3,5- trimethoxybenzene)

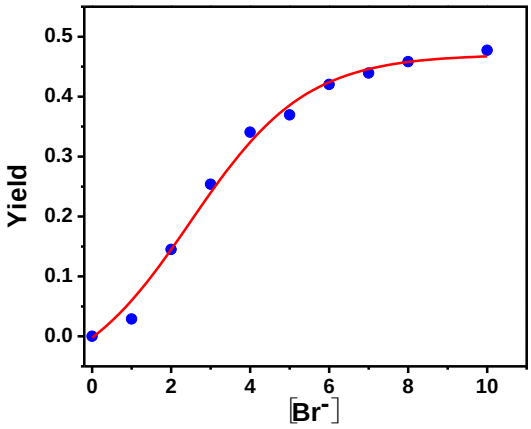

Figure S66. The fitting curve of the yield with different equiv of Br^- anions.

7.2 Titration of Tet-1 with NBu_4I

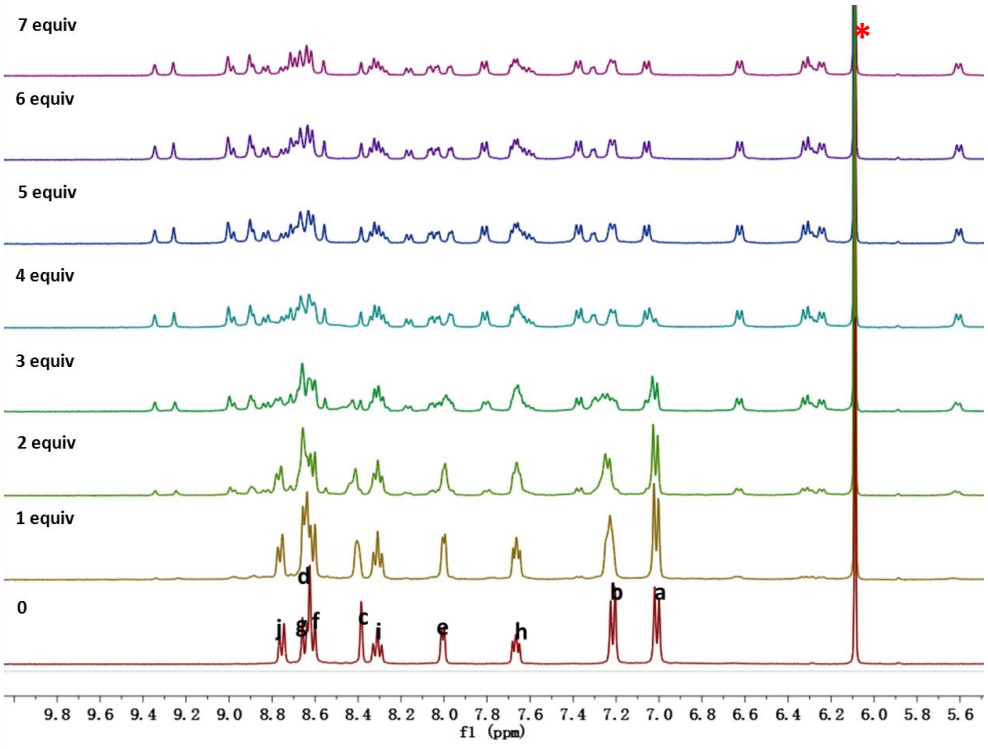

Figure S67. ^1H NMR spectra following the titration of Bu_4NI into **Tet**-1 (CD_3CN, 400 MHz) and recorded immediately at 298K. The equivalents of I^- are indicated on the left side of the spectra. (* was label as the internal standard 1,3,5- trimethoxybenzene)

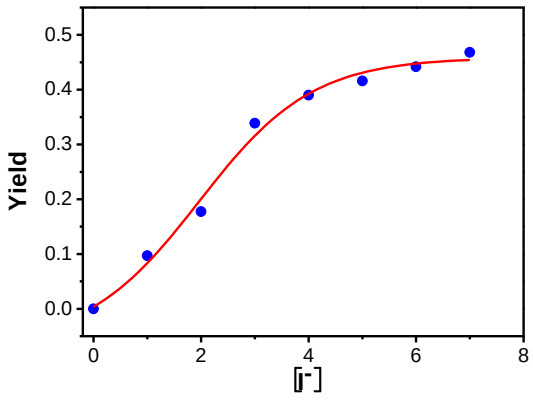

Figure S68. The fitting curve of the yield of Cat-I with different equiv of I^- anions.

8. Isothermal titration calorimetry (ITC) measurement

The ITC experiments were performed by an isothermal titration microcalorimeter at atmospheric pressure and at 25 ℃ in CH_3CN solution, giving the association constants (K) and the thermodynamic parameters of Br^- upon complexation with **Tet**-1. A solution of Bu_4NBr or Bu_4NI in a 0.250 mL syringe was sequentially injected with stirring at 300 rpm into a solution of tetrahedron **Tet**-1 in the sample cell (1.00 mL volume). All the thermodynamic parameters reported in this work were obtained by using the "independent" model in Nanoanalyze software of Nano ITC instrument.

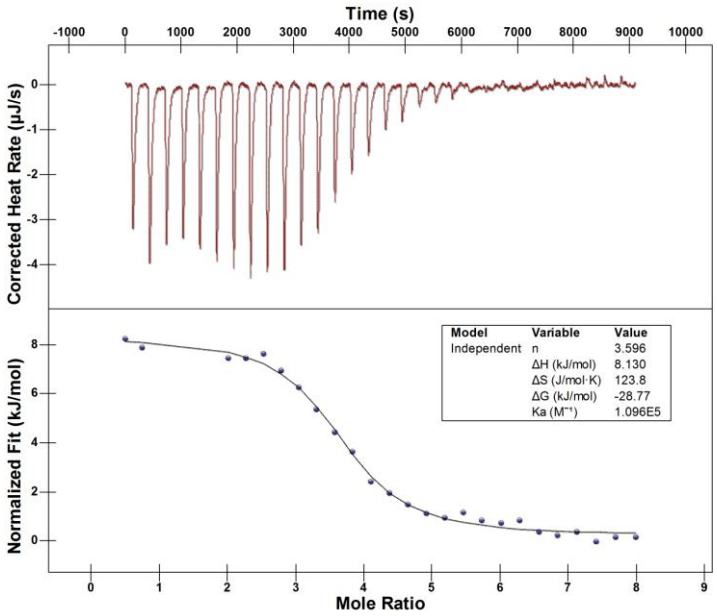

Figure S69. Raw data and apparent reaction heat of the isothermal titration calorimetry for sequential injections (10 μL per injection) of Br^- solution (5 mM) injecting into **Tet**-1 solution (0.125 mM).

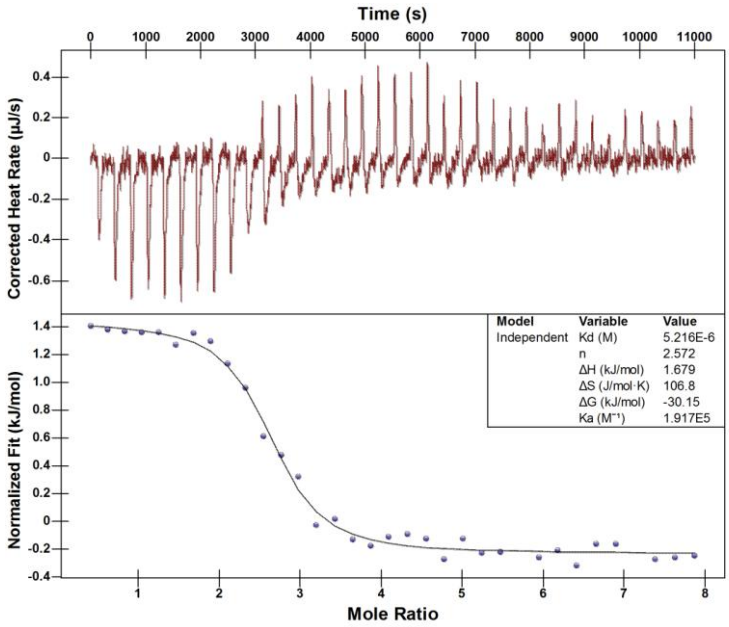

Figure S70. Raw data and apparent reaction heat of the isothermal titration calorimetry for sequential injections (5 μL per injection) of I^- solution (5 mM) injecting into **Tet**-1 solution (0.125 mM).

Table S4. Summary of the association constants and thermodynamic parameters

	n	ΔH(kJ/mol)	ΔS(kJ/mol)	ΔG(kJ/mol)	Ka(M^{-1})
Br^-	3.5±0.064	8.13±0.4	123.8	-28.77	1.096E5
I^-	2.6±0.06	1.68±0.08	106.8	-30.15	1.917E5

9. The reversible unlock/interlock process with the titration of Ag^+ ions

General procedure

To a solution of the halide filled interlocked cage **Cat**-X (500 μL, 2 mM, CD3CN), a silver(I) salt solution (CD_3CN, 0.1 M) was added in steps of 1.0 equiv (10 μL). The NMR spectrum was recorded after each addition and the sample was mixed thoroughly before each measurement.

9.1 Titration of interlocked cage Cat-Br with $AgCF_3SO_3$

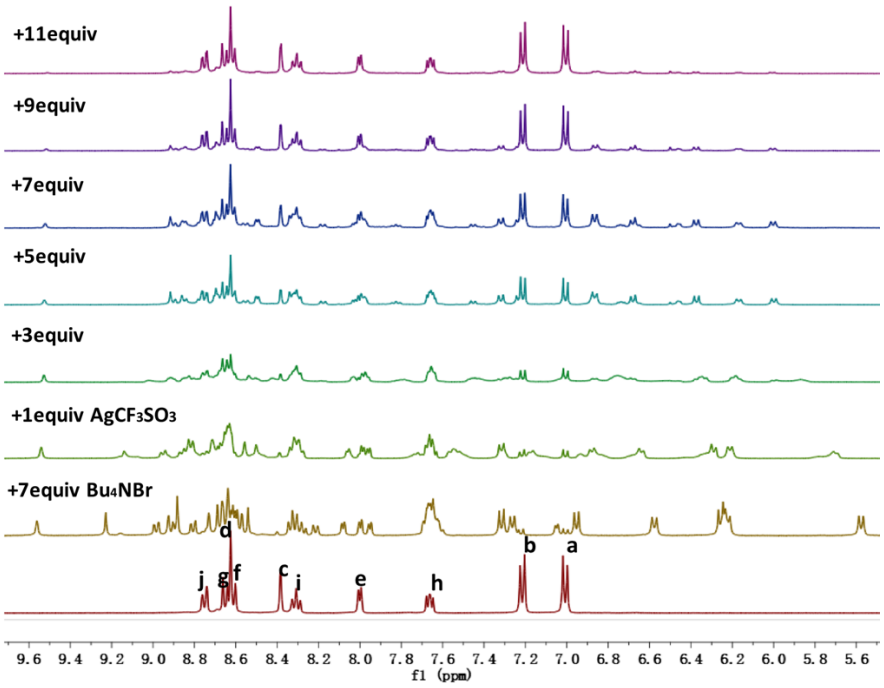

Figure S71. ^1H NMR spectra following the titration of $AgCF_3SO_3$ into cage **Cat**-Br $[Zn_8L_8][Br]_7$ (CD_3CN, 400 MHz) and recorded immediately at 298K. The equivalents of Ag^+ are indicated on the left side of the spectra. The formation of new peaks was due to the precipitation of AgBr and unlocked the interlocked cage.

9.2 Titration of interlocked cage Cat-I with $AgCF_3SO_3$

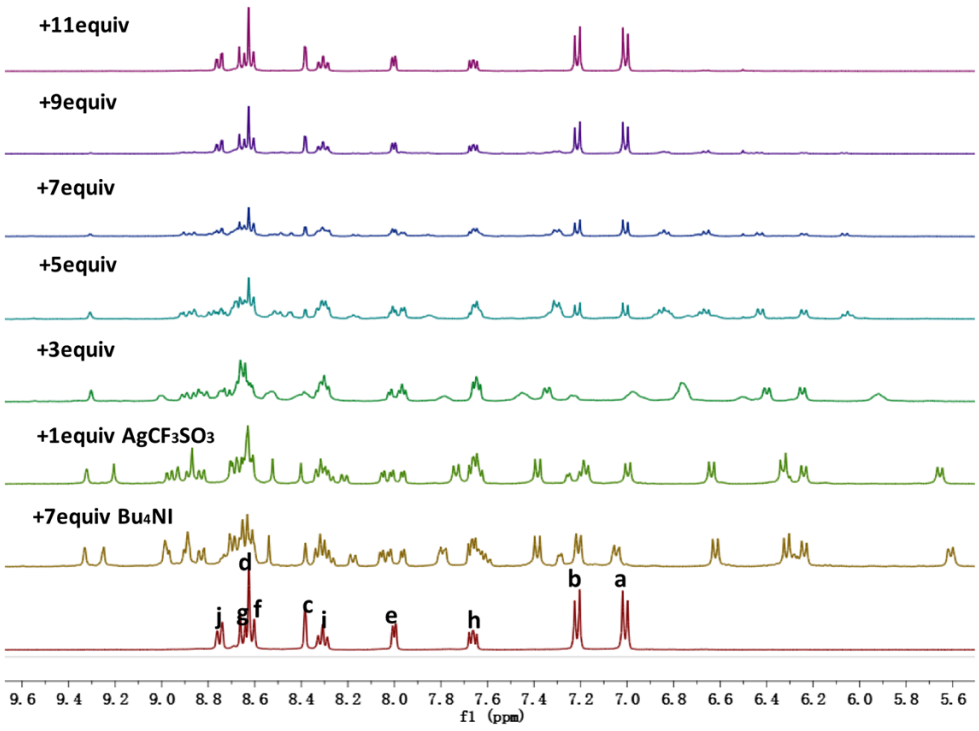

Figure S72. ^1H NMR spectra following the titration of $AgCF_3SO_3$ into cage **Cat**-I $[Zn_8L_8][I]_7$ (CD_3CN, 400 MHz) and recorded immediately at 298K. The equivalents of Ag^+ are indicated on the left side of the spectra. The formation of new peaks was due to the precipitation of AgI and unlocked the interlocked cage.

9.3 Titration of interlocked cage Cat-Br with MeOTf

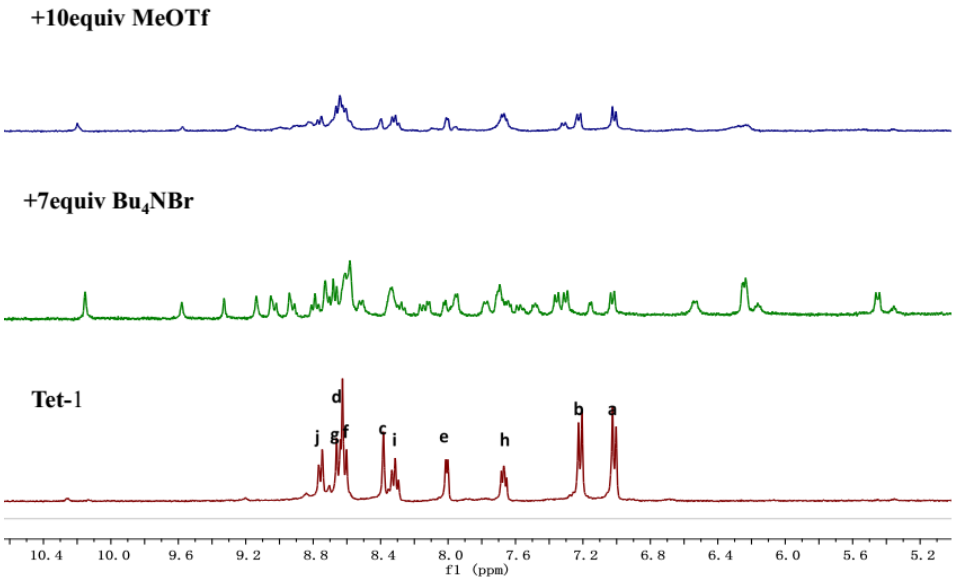

Figure S73. ^{1}H NMR spectra following the titration of MeOTf into cage **Cat**-Br $[Zn_8L_8][Br]_7$ (CD_3CN, 400 MHz) and recorded immediately at 298K. The formation of new peaks was due to the abstract of Br^- and unlocked the interlocked cage.

10. Emission Spectra titration data for host-guest complex

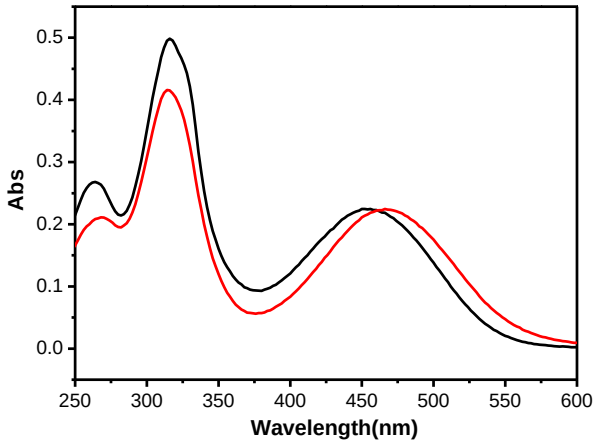

Figure S74. Family of UV-vis absorption spectra of **Tet**-1 (red line) and interlocked cage **Cat-BF4** (black line) in CH_3CN.

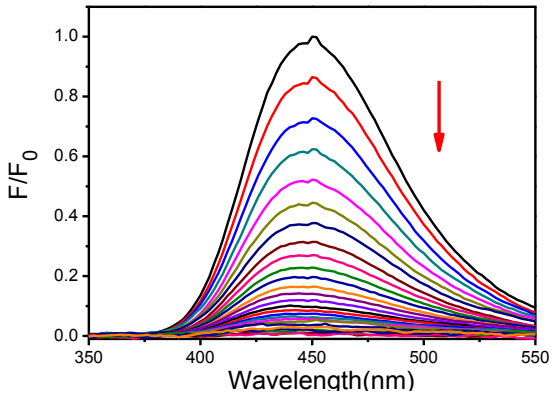

Figure S75. Fluorescence spectra of Bu_4N**DSA** (10 μM) in CH_3CN upon addition of 1 equiv **Tet**-1 up to 10 μM.

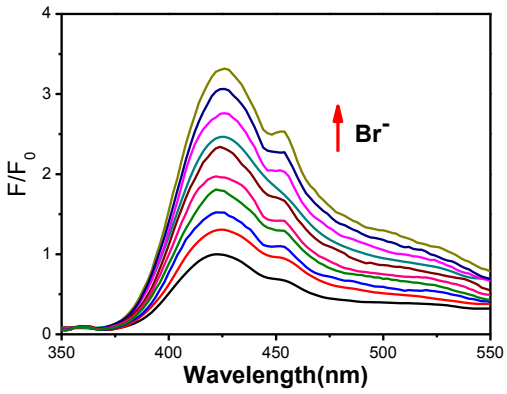

Figure S76. Fluorescence spectra of Bu_4N**DSA** (10 μM) in CH_3CN upon addition of 1 equiv **Tet**-1 (black line) with the titration of Bu_4NBr

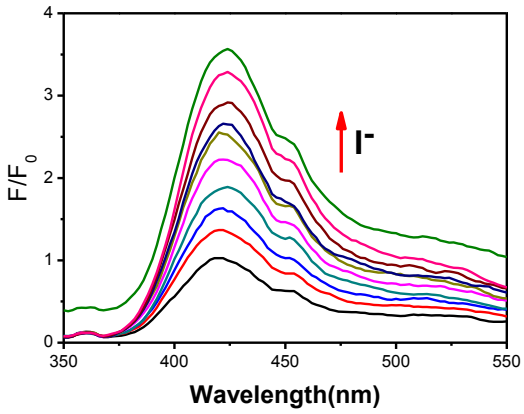

Figure S77. Family of fluorescence of Bu_4N**DSA** (10 μM) in CH_3CN upon addition of 1 equiv **Tet**-1 (black line) with the titration of Bu_4NI.

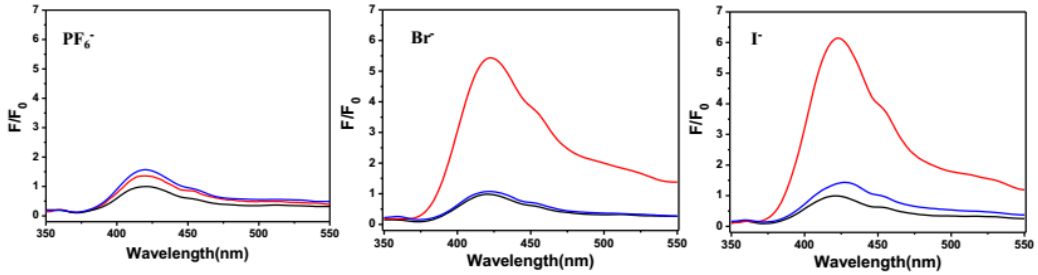

Figure S78. Family of fluorescence of Bu_4N**DSA** (10 μM) in CH_3CN in presence of 1 equiv of **Tet**-1 (black line) with the addition of 10 equiv of template ions (PF_6^-, Br^-, I^-) (red line), and subsequently titration of 20 equiv of **$AgCF_3SO_3$** (blue line). Only Br^- and I^- template systems showed clear fluorescence quenching recovery process corresponding to the interlocked reversible process.

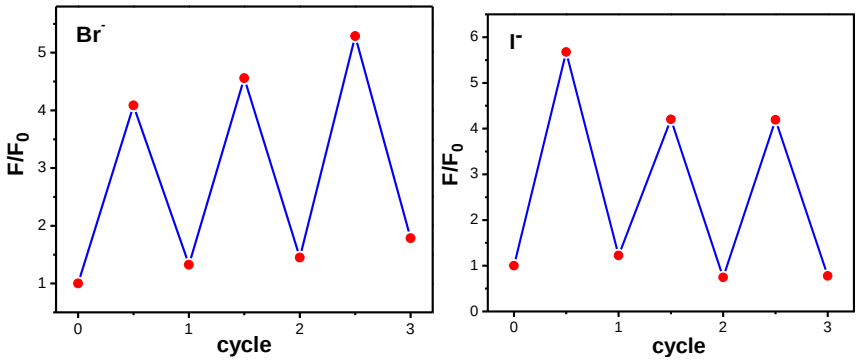

Figure S79. Normalization fluorescence spectra of Bu_4N**DSA** (10 μM) in CH_3CN in presence of 1 equiv of **Tet**-1 with the addition of 20 equiv of Br^- (left) or I^- (right), and subsequently titration of 20 equiv of $AgCF_3SO_3$ and recycle use for three times. The slight weaken of the fluorescence with addition of I^- may be due to the little turbidity of the host-guest complex solution.

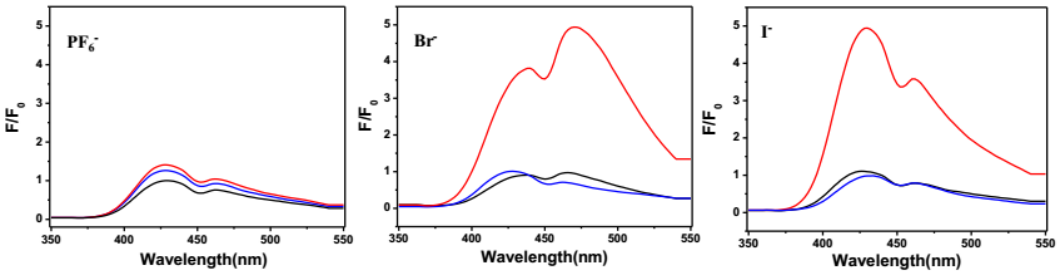

Figure S80. Fluorescence of Bu_4N**DSA** (10 μM) in CH_3CN in presence of 1 equiv of **Tet**-1 (black line) with the addition of 10 equiv of template ions (PF_6^-, Br^-, I^-) (red line), and subsequently titration of 20 equiv of **MeOTf** (blue line). Br^- and I^- template systems showed clear fluorescence quenching recovery process corresponding to the interlocked reversible process.

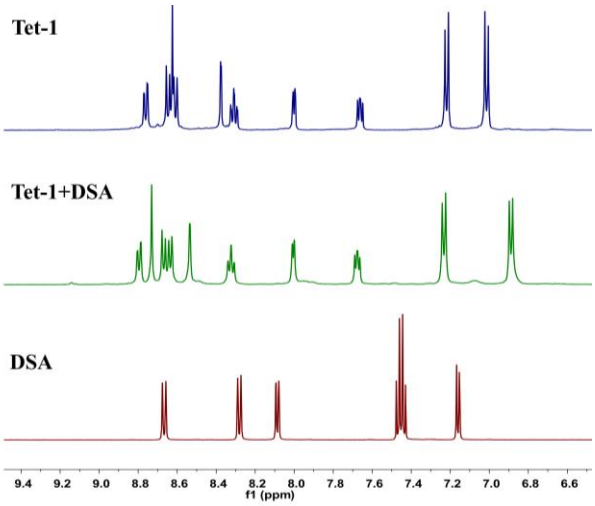

Figure S81. ^{1}H NMR spectrum of **Tet**-1 upon addition of 5 equiv. of **DSA.** The chemical shift changes of Ha, Hc and Hd indicated the formation of complex **DSA⊂Tet**-1.

11. The dehalogenation reaction of bromohydrocarbons with Tet-1

General procedure

Mixing the discrete cage **Tet-1** (1 mM), 3-bromocyclohexene (10 equiv), 2, 4, 6-collidine (20 equiv) and MeOTf (20 equiv) in a CH_3CN solution, the reaction was stirred at room temperature for 3 h. The concentration of the substrates was calculated by the internal standard.

Control experiment was carried out following the procedure described above with the difference of catalyst. The conversion was shown in Table S5.

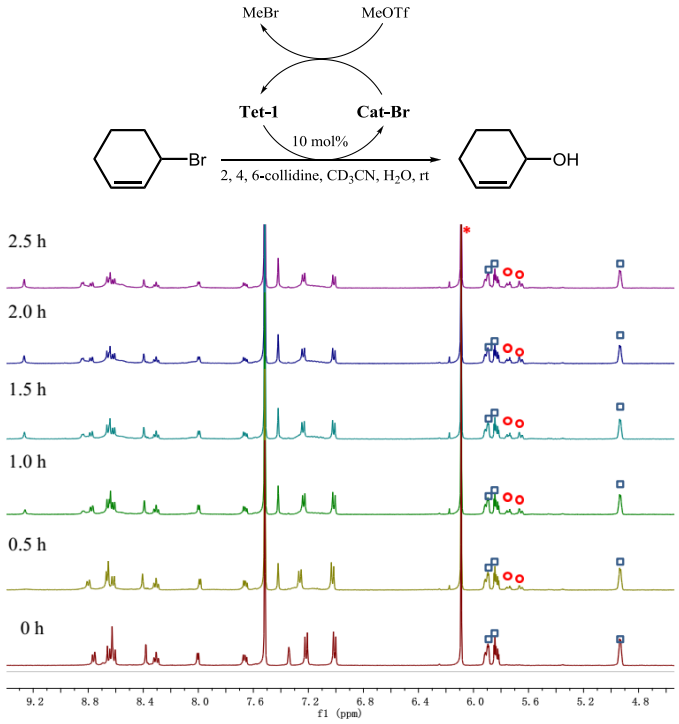

Figure S82. ^1H NMR (CD_3CN, 500 MHz) monitoring the dehalogenation reaction of 3-bromocyclohexene, with system containing 2, 4, 6-collidine (20 mM), MeOTf (20 mM) and **Tet**-1 fixed at 0.5 mM, showing the increasing tendency of the peaks on the products (red cycle), while the gradual vanish of the substrate (blue square), with the proceeding of the reaction. (* was label as the internal standard 1,3,5- trimethoxybenzene).

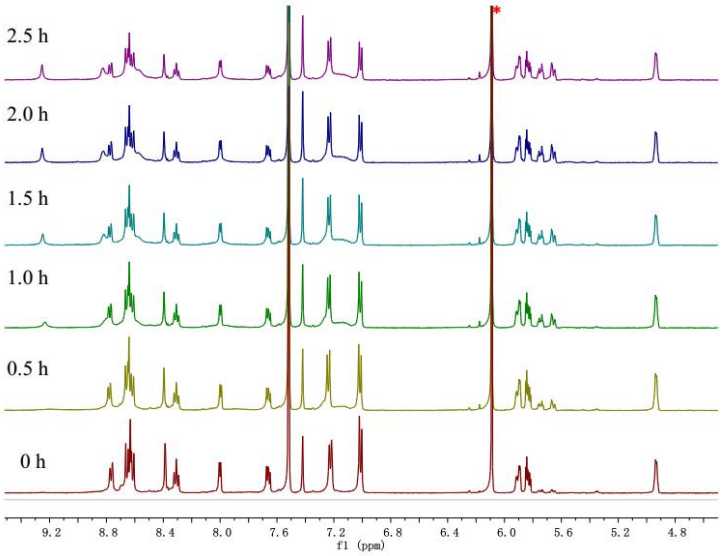

Figure S83. ^{1}H NMR (CD_3CN, 500 MHz) monitoring the dehalogenation reaction of 3-bromocyclohexene (10 mM), with system containing 2, 4, 6-collidine (20 mM), MeOTf (20 mM) and **Tet**-1 (1 mM). (* was label as the internal standard 1,3,5- trimethoxybenzene).

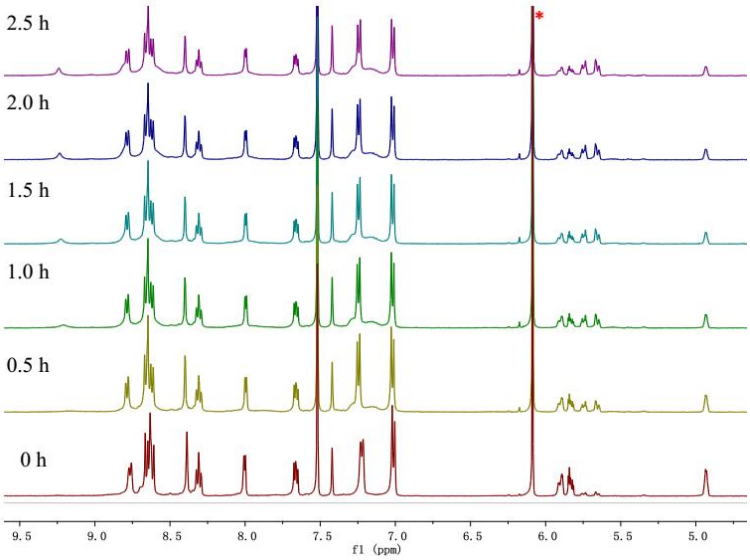

Figure S84. ^{1}H NMR (CD_3CN, 500 MHz) monitoring the dehalogenation reaction of 3-bromocyclohexene (10 mM), with system containing 2, 4, 6-collidine (20 mM), MeOTf (20 mM) and **Tet**-1 (1.5 mM). (* was label as the internal standard 1,3,5- trimethoxybenzene).

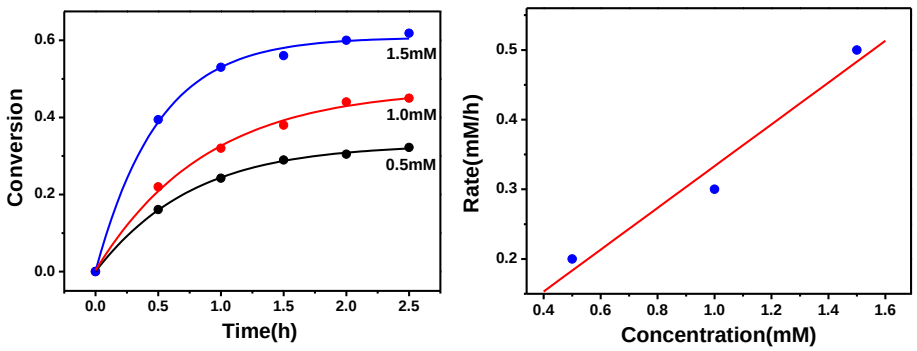

Figure S85. (Left) Conversion of the dehalogenation of 3-bromocyclohexene (10.0 mM) of system containing 2, 4, 6-collidine (20 mM), MeOTf (20 mM), and different concentration of **Tet**-1 in a CD_3CN solution. (Right) The picture showing the initial rate vs. concentration of the tetrahedron **Tet**-1.

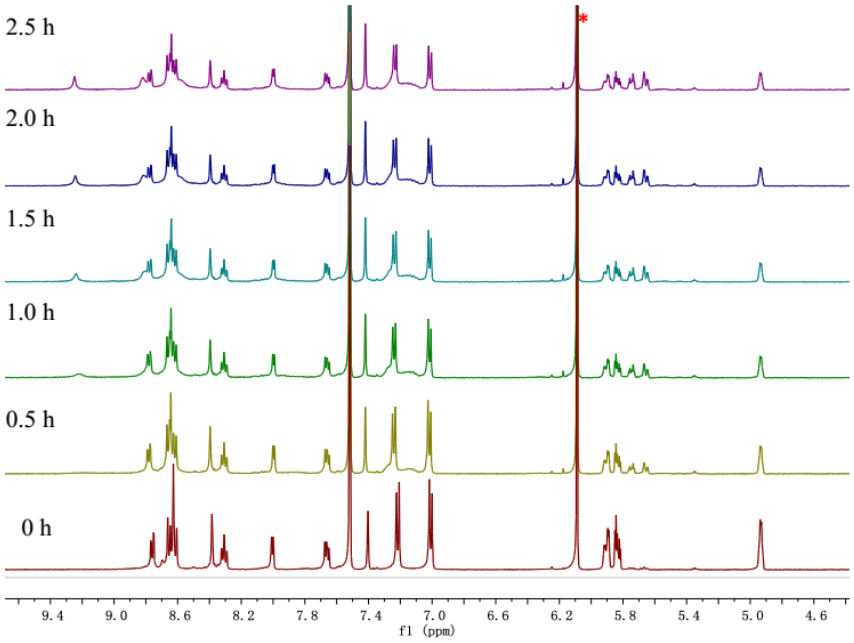

Figure S86. ^1H NMR (CD_3CN, 500 MHz) monitoring the dehalogenation reaction of 3-bromocyclohexene (7.5 mM), with system containing 2, 4, 6-collidine (20 mM), MeOTf (20 mM) and **Tet**-1 (1.0 mM). (* was label as the internal standard 1,3,5- trimethoxybenzene).

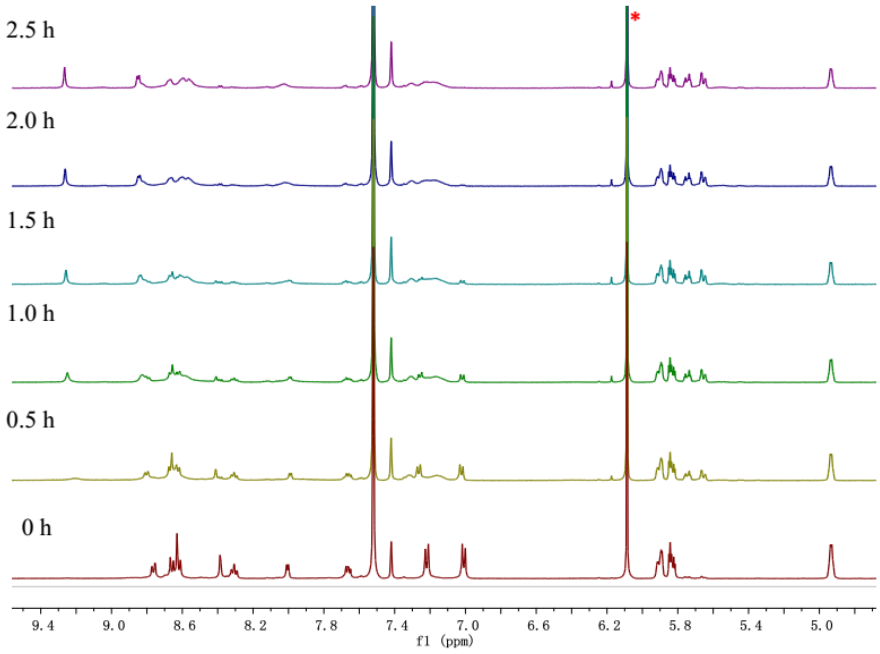

Figure S87. ^{1}H NMR (CD_3CN, 500 MHz) monitoring the dehalogenation reaction of 3-bromocyclohexene (12.5 mM), with system containing 2, 4, 6-collidine (20 mM), MeOTf (20 mM) and **Tet**-1 (1.0 mM). (* was label as the internal standard 1,3,5- trimethoxybenzene).

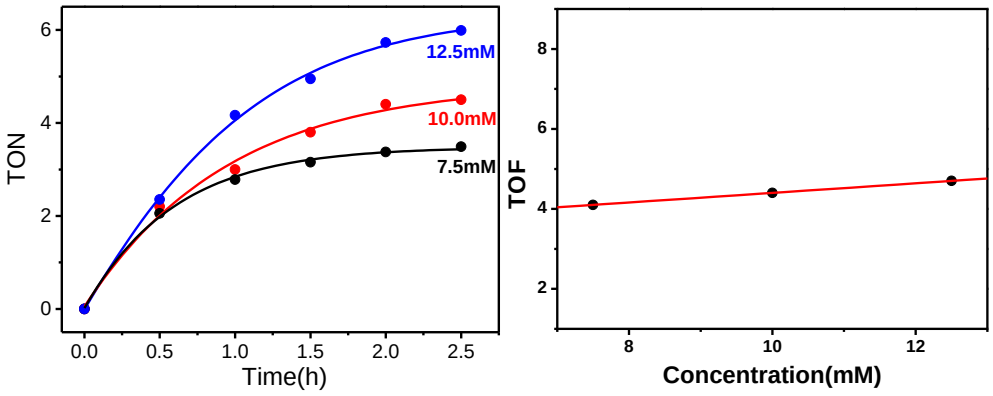

Figure S88. (Left) TON of the dehalogenation reaction of different concentration of 3-bromocyclohexene by the system containing 2, 4, 6-collidine (20 mM), MeOTf (20 mM), and **Tet**-1 (1 mM) in a CD_3CN solution. (Right) The picture showing the initial TOF vs. concentration of the substrate.

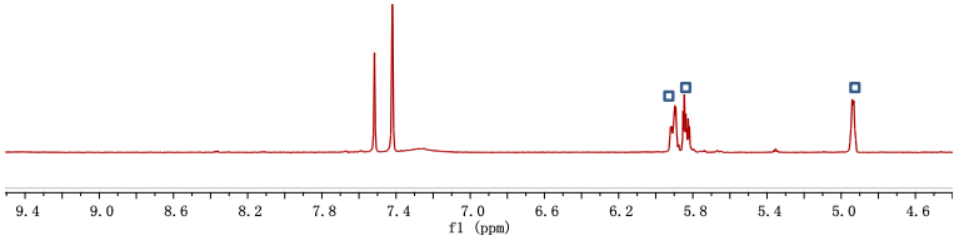

Figure S89. Control experiment of dehalogenation reaction of 3-bromocyclohexene (10 mM) by the system containing 2, 4, 6-collidine (20 mM), MeOTf (20 mM) in the absence of **Tet**-1. No corresponding product was detected.

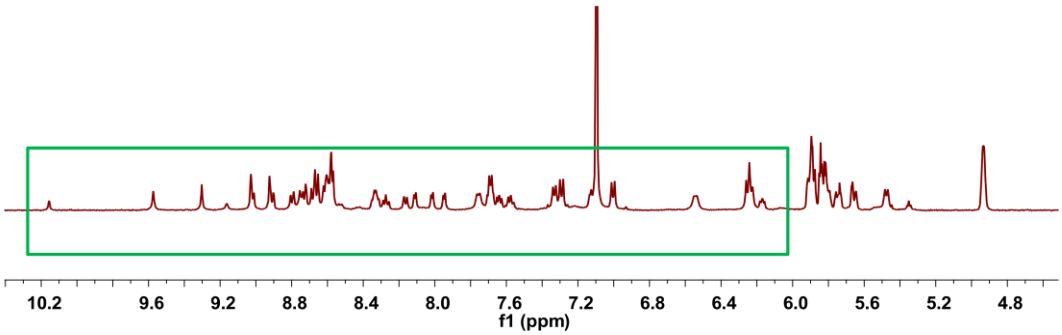

Figure S90. Control experiment of dehalogenation reaction of 3-bromocyclohexene (20 mM) by the system containing 2, 4, 6-collidine (20 mM), **Tet**-1 (1 mM) in the absence of MeOTf. The new peaks corresponding to Cat-Br appeared. It was shown that **Tet**-1 can be converted into Cat-Br in the presence of the stoichiometric amount of 3-bromocyclohexene.

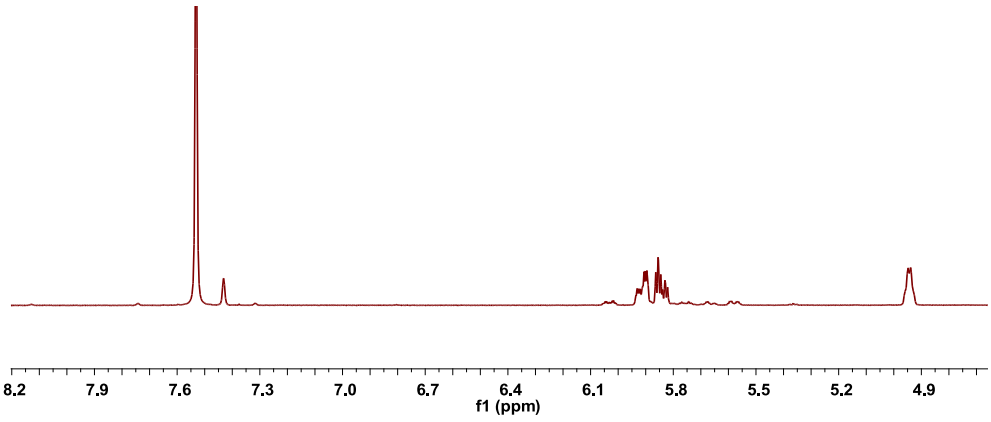

Figure S91. Control experiment of dehalogenation reaction of 3-bromocyclohexene (10 mM) by the system containing 2, 4, 6-collidine (20 mM), $Zn(OTf)_2$ (4 mM) and MeOTf (20 mM).

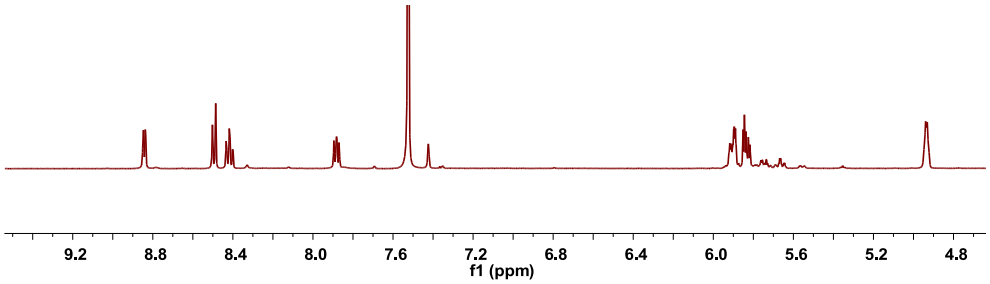

Figure S92. Control experiment of dehalogenation reaction of 3-bromocyclohexene (10 mM) by the system containing 2, 4, 6-collidine (20 mM), $Zn(bpy)_3(CF_3SO_3)_2$ (4 mM) and MeOTf (20 mM).

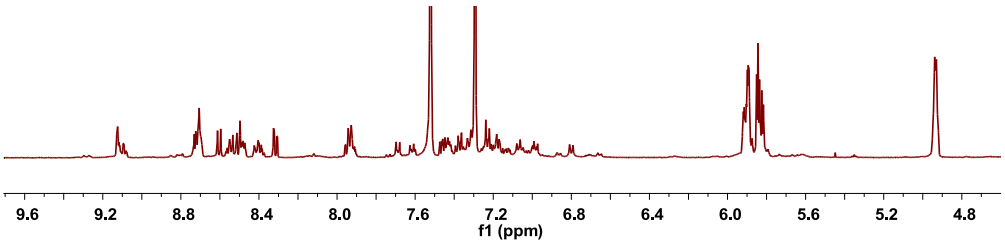

Figure S93. Control experiment of dehalogenation reaction of 3-bromocyclohexene (10 mM) by the system containing 2, 4, 6-collidine (20 mM), ligand L (4 mM TPA+ 2,2'-bipyridine-5-carbaldehyde, pre-refluxing in CD_3CN for 5h) and MeOTf (20 mM).

Table S5. Summary of the conversion of the control experiments.

Entry	**Catalyst(X mol%)**	**Conversion(%)**
1	-	0
2	L(40)	0
3	$Zn(OTf)_2$(40)	3
4	$Zn(bpy)_3(OTf)_2$(40)	12
5	**Tet**-1(10)	65

Notes and references

(1) M. Otte, P. F. Kuijpers, O. Troeppner, I. Ivanovic-Burmazovic, J. N. H. Reek and B. Bruin, *Chem. Eur. J.*, 2013, **19**, 10170.

(2) B. Tzeng, A. Chao, T. Selvam and T. Chang, *CrystEngComm*, 2013, **15**, 5337.

(3) SMART Data collection software, version 5.629; Bruker AXS Inc.: Madison, WI, 2003.

(4) SAINT Data reduction software, version 6.45; Bruker AXS Inc.: Madison, WI, 2003.

(5) Sheldrick, G. M. SHELX-97: Program for crystal structure analysis; University of Göttingen: Göttingen, Germany, 1997.

(6) Spek, A. L. PLATON, University of Glasgow, Glasgow (Scotland)**,** 1998**.**